博士論文

Autophagy adaptors mediate Parkin-dependent mitophagy by forming sheet-like liquid condensates

(マイトファジー時におけるシート状液滴の研究)

楊　　梓
Yang Zi

Autophagy adaptors mediate Parkin-dependent mitophagy by forming sheet-like liquid condensates

Affiliation: Department of Biochemistry and Molecular Biology, Graduate School of Medicine, The University of Tokyo, Tokyo 113-0033, Japan

Supervisor: Noboru Mizushima

Yang Zi

Contents

Pages

Abbreviations.....4

Abstract.....6

Introduction.....7

Materials and Methods.....13

Results.....19

Discussion.....26

References.....30

Table.....43

Figures.....44

Acknowledgements.....65

Abbreviations

OPTN: Optineurin

NDP52/CALCOCO2: Calcium binding and coiled-coil domain 2

BSA: Bovine serum albumin

p62/SQSTM1: Sequestosome 1

NBR1: Next to BRCA1 gene 1 protein

TAX1BP1: Tax1 binding protein 1

PB1: Phox and Bem1 domain

UBD: Ubiquitin-binding domain

LIR: LC3-interacting region

LLPS: Liquid-liquid phase separation

CCCP: Carbonyl cyanide m-chlorophenylhydrazone

Penta KO: Penta knock out

FRAP: Fluorescence recovery after photobleaching

PASs: Pre-autophagosomal structures

GFP: Green fluorescent protein

DMEM: Dulbecco's modified Eagle's medium

DMSO: Dimethyl sulfoxide

FBS: Fetal bovine serum

HRP: Horseradish peroxidase

HEK: Human Embryonic Kidney cells

EDTA: Ethylenediaminetetraacetic acid

HEPES: 4-(2-hydroxyethyl)-1-piperazineethanesulfonic acid

PBS: Phosphate-buffered saline

SDS-PAGE: Sodium dodecyl sulfate-poly-acrylamide gel electrophoresis

SF650: HaloTag ligand SaraFluor 650T

TBST: Tris-buffered saline with Tween-20

Abstract

During PINK1 and Parkin-mediated mitophagy, autophagy adaptors are recruited to depolarized mitochondria to promote the selective degradation of mitochondria. Autophagy adaptors such as OPTN and NDP52 bridge mitochondria and autophagosomal membranes by binding to ubiquitinated mitochondrial proteins and autophagosomal ATG8 family proteins. Here, I demonstrate that OPTN and NDP52 form sheet-like phase-separated condensates with liquid-like properties on the surface of ubiquitinated mitochondria. The dynamic and liquid-like feature of OPTN condensates is important for mitophagy activity because reducing the liquidity of OPTN–ubiquitin condensates suppresses the recruitment of ATG9 vesicles and impairs mitophagy. Based on these results, I propose a dynamic liquid-like model of autophagy adaptors, in contrast to a stoichiometric model, to explain their interactions between autophagic membranes (i.e., ATG9 vesicles and isolation membranes) and mitochondrial membranes during Parkin-mediated mitophagy. This model underscores the importance of liquid–liquid phase separation in facilitating membrane–membrane contacts, likely through the generation of capillary forces.

Keywords

autophagy; mitophagy; liquid–liquid phase separation; optineurin; wetting

Introduction

Autophagy

Macroautophagy (hereafter referred to as autophagy) is an intracellular degradation process that is well-conserved throughout the eukaryotes and an essential pathway to maintain cellular homeostasis[1-3]. During this process, various cytosolic components, including proteins and organelles, are sequestered into double-membrane vesicles called ‘autophagosomes’[3]. In the process of autophagosome formation, a small membrane structure known as the "isolation membrane" or "phagophore" emerges in the cytoplasm (Fig. 1A). The isolation membrane expands and forms a double membraned organelle, an autophagosome. Subsequently, the autophagosome fuses with the lysosome in mammalian cells or the vacuole in yeast and plant cells, resulting in the formation of the autolysosome (mammalian cells) or autophagic body (yeasts/plants). With various hydrolases in these organelles, the inner autophagosomal membrane and the materials it encloses are broken down. The resulting degradation products are then transported back to the cytoplasm, where they are recycled for various cellular functions (Fig. 1A)[3-7].

Autophagy was originally considered as a non-selective, bulk degradation pathway responding to nutrient starvation; however, it has become well-established that it can also be selective[8, 9]. Selective autophagy is responsible for the targeted degradation of specific intracellular components, such as protein aggregates (aggrephagy), organelles including endoplasmic reticulum (ER) (ER-phagy),

lysosome (lysophagy), intracellular pathogens (xenophagy), and mitochondria (mitophagy)[10-14]. Autophagy adaptors or receptors participate in recognition of selective autophagy substrates (Fig. 1B). Autophagy adaptors are soluble proteins responsible for bridging cargoes and autophagy machinery, while autophagy receptors are cargo-resident proteins that interact with the autophagy machinery. Among the autophagy adaptors, SQSTM1/p62 (sequestosome 1) is involved in aggrephagy and lysophagy[15, 16], while optineurin (OPTN) and CALCOCO2/NDP52 are required for xenophagy and mitophagy[17, 18]. These autophagy adaptors bind to ubiquitinated cargoes through their ubiquitin-binding domains. Examples of autophagy receptors include TEX264 for ER-phagy[19] and NIX/BNIP3 for mitophagy[20]. Both autophagy adaptors and receptors contain LC3 interaction regions (LIRs) to facilitate binding with ATG8/LC3 family proteins (Fig. 1B)[9].

Mitochondria and mitophagy

Mitochondria are a double-membraned organelle that plays essential roles in eukaryotic cells by generating adenosine triphosphate through oxidative phosphorylation. They also participate in crucial cellular processes such as β-oxidation, cell signaling, apoptosis, and calcium homeostasis[21-24]. While acting as the cellular powerhouses, mitochondria generate reactive oxygen species (ROS) as byproducts, making them particularly susceptible to oxidative damage[25-27]. Damaged mitochondria, characterized by a loss of membrane potential, can become significant sources of ROS production. To counter this risk and maintain a healthy

and functional mitochondrial network, cells have developed mechanisms to repair and eliminate damaged components or remove the entire dysfunctional mitochondria by selective autophagy called mitophagy[28].

Mitophagy specifically degrades damaged mitochondria and can be induced by mitochondrial damage or cellular stresses[14, 29]. Several papers have shown that mitophagy occurs under various stress conditions. For example, after losing the mitochondrial membrane potential, numerous mitochondrial outer-membrane proteins are ubiquitinated by the PINK1-Parkin system. PINK1 is a protein kinase that accumulates on the outer membrane of impaired mitochondria with diminished membrane potential. When PINK1 is stabilized, it gains the ability to phosphorylate multiple downstream targets, such as the E3 ubiquitin ligase Parkin and ubiquitin itself[30, 31]. Activated Parkin by PINK1, in turn ubiquitinates mitochondrial outer membrane proteins, which sets off a series of molecular events, such as initiating the recruitment of autophagy adaptors, OPTN, NDP52, p62, NBR1 (Next to BRCA1 gene 1 protein), and TAX1BP1 (Tax1 binding protein 1)[8, 9, 18, 31, 32] (Fig. 1B and C). These autophagy adaptors bridge the mitochondrial and autophagosomal membranes by interacting with mitochondrial ubiquitinated proteins via a ubiquitin-binding domain (UBD) and with autophagosomal ATG8 family proteins (i.e., LC3 and GABARAP family proteins in mammals) via the LIR domain (Fig. 1B and C). In addition to their role in bridging mitochondria and autophagosomes, autophagy adaptors play different roles during mitophagy. p62 causes mitochondrial clustering and OTPN and NDP52 play crucial roles in inducing mitophagy by recruiting

upstream autophagy factors[33, 34]. OPTN recruits ATG9 vesicles, whereas NDP52 recruits the ULK1 complex through interaction with FIP200[9, 35].

Liquid-liquid phase separation

Liquid–liquid phase separation (LLPS) has been described in various biological processes[36-39] as a powerful mechanism to explain the formation of membraneless organelles and their essential roles in cellular processes[40-43]. LLPS involves the formation of liquid-like condensates through dynamic, multivalent interactions between various molecules that often possess intrinsically disordered regions, which show higher protein concentration and weaker molecular mobility than the surrounding medium facilitating higher biochemical reactions [39, 44, 45]. Emerging evidence suggests connections between autophagy and LLPS at multiple steps, including autophagosome formation and degradation[46, 47]. Notably, autophagy adaptors, such as p62, undergo LLPS through multivalent interaction with poly-ubiquitin and form cytosolic condensates[48, 49]. p62 undergoes phase separation, which depends on several factors, including self-interaction through the Phox and Bem1 (PB1) domain, its interaction with ubiquitin via the UBA domain, and the valence of the poly-ubiquitin chains[48, 50] (Fig. 2). Moreover, p62 directly binds to ATG8 family proteins on the isolation membrane through its LIR domain. These interactions enable efficient engulfment of p62 condensates by autophagosomes and their subsequent degradation, a process called “fluidophagy” (Fig. 2)[51]. Furthermore, recent studies showed that p62 undergoes LLPS on mitochondria and

lysosomes that are subjected to selective autophagy. p62 and heat shock protein HSP27 facilitate lysophagy via the formation of phase-separated condensates[52]. HSP27 has been reported to prevent gelation and sustain the fluidity of p62, thereby facilitating the efficient lysophagy. Similarly, another p62 binding protein, Nur77, has been reported to modulate the liquidity of p62 condensates during celastrol-induced mitophagy[52, 53].

Generally, phase-separated condensates can deform when they contact a rigid surface to minimize the overall energy of the system, a phenomenon known as "wetting" (Fig. 3A)[54, 55]. The wetting behavior of intracellular condensates is determined by the interfacial tensions between the condensate–membrane, condensate–cytosol, and cytosol-membrane interfaces. Depending on the relative strengths of these interfacial tensions, the condensates exhibit or no-wetting, partial wetting, or complete wetting (Fig. 3A)[54]. In contrast, elastic surfaces, including membranes to which phase-separated condensates adhere, also deform (Fig. 3B)[54-56]. This indeed happens during fluidophagy; autophagosomal membranes bend along the surface of p62 condensates[51]. The deformation of a membrane by a phase-separated condensate is determined by the energy balance between membrane deformation and the surface tension of the condensate, which is known as elasto-capillarity[54, 57].

Purpose of this study

By forming capillary bridges, wetting droplets can also induce adhesion of surfaces[58]. Whether LLPS and capillary bridges also contribute to the adhesion of cellular membranes is not presently known. In this study, I employed live-cell imaging to provide evidence that the autophagy adaptors form phase-separated condensates on the surface of the mitochondrial membrane. In contrast to the classical spherical droplets formed in the cytosol, the condensate formed by OPTN is more like a flat, broad, and thin sheet covering the surface of the damaged mitochondrial membrane upon mitophagy induction. We call this the “sheet-like condensate.” These condensates accumulate between mitochondria or between mitochondria and autophagic membranes, exhibiting a dynamic nature with a liquid-like property. Furthermore, I demonstrate the essential role of these dynamic condensates in the recruitment of ATG9 vesicles and the initiation of mitophagy. Based on these results, I suggest a departure from the current stoichiometric model, where autophagy adaptors bind to ubiquitin at one end through their ubiquitin binding domain and, at the other end, bind to LC3 by LIR motif, forming a one-to-one binding structure. Instead, I propose a dynamic liquid-like model to describe the roles of autophagy adaptors in Parkin-mediated mitophagy and discuss the hypothesis that phase-separated condensates of autophagy adaptors can wet both mitochondria and autophagic membranes, including ATG9 vesicles and isolation membranes (also called phagophores), thereby promoting their contact during Parkin-mediated mitophagy.

Materials and Methods

Cell culture

HeLa cells, HeLa penta-knockout (penta KO) cells, and human embryonic kidney (HEK) 293T cells authenticated by RIKEN were cultured in Dulbecco's modified Eagle's medium (DMEM; D6546; Sigma-Aldrich) supplemented with 10% fetal bovine serum (FBS; 173012; Sigma-Aldrich) and 2 mM L-glutamine (25030-081; Gibco) in a 5% CO_2 incubator at 37°C.

Retrovirus production and generation of stable cell lines

HEK 293T cells at 60% confluency were transfected with 1.8 μg retroviral vector carrying the gene of interest, 0.9 μg pCG-VSV-G, 0.9 μg pCG-gag-pol (gifts from Dr. T. Yasui, National Institutes of Biomedical Innovation, Health and Nutrition), and 2 μl Lipofectamine 2000 (11668019; Thermo Fisher Scientific) transiently. DNA mixture and Lipofectamine were mixed and incubated for 10 min at 25 ℃ after 5 min prior incubation with 200 μl OPTI-MEM (31985070; Thermo Fisher Scientific). After adding the mixture for 16 h, the medium was replaced with DMEN. After transfection, cells were further incubated at 37°C for 24h. The viral supernatant was collected by filtration through a 0.45-μm filter unit (Ultrafree-MC; Millipore) and then used for infection. Cells were plated onto 6-cm dishes 18 h before infection, and the medium was replaced with viral supernatant diluted 1.5-fold with 8 μg/mL polybrene (H9268; Sigma-Aldrich). Two days later, cells were selected in a medium

containing 2 μg/mL puromycin (P8833; Sigma-Aldrich), 4 μg/mL blasticidin S hydrochloride (022-18713; FUJIFILM Wako Pure Chemical Corporation), 1.5 mg/mL neomycin, or 250 μg/mL zeocin (R25005; Thermo Fisher Scientific).

Plasmids

The pMRX-IPU, pMRX-IBU, and pMRX-INU plasmids were generated by modifying the multi-cloning site of pMRX-IP[59, 60], pMRX-IB, and pMRX-IN, respectively. DNA fragments encoding ubiquitin, p62 (NM_003900.5), OPTN (NM_001008211.1), NBR1 (NM_001291571.2), NDP52 (NM_001261391.2), TAX1BP1 (NM_001206901.1), ATG9A (NM_001077198.3), LC3A (NM_032514.4), and LC3B (NM_022818.5) were inserted into pMRX-IPU, pMRX-INU, or pMRX-IBU. DNAs encoding the HA epitope, monomeric enhanced GFP with the A206K mutation (mGFP), codon-optimized ultra-stable GFP (muGFP)[61], codon-optimized mRuby3[62], HaloTag7 (G1891; Promega), 3×FLAG, and SNAP-tag (New England BioLabs, N9181S) were used for tagging. The mitochondrial presequence of *Neurospora crassa* Fo-ATPase subunit 9 (residues 1–69) was added to HaloTag7-SNAP to deliver the reporter into the mitochondrial matrix (mtHalo-SNAP). SNAP-tag was added to increase the size of protein [63]. Truncated OPTN (OPTNΔUBAN, aa 445–502) was prepared by PCR-mediated site-directed mutagenesis. Used primers are listed in Table 1. The resulting plasmids were sequenced.

Antibodies and reagents

The primary antibodies used in this study were rabbit polyclonal anti-OPTN (Proteintech, 10837-AP), rabbit polyclonal anti-ATG9A (MBL, PD042), mouse monoclonal anti-Halo (Promega, G9211), mouse monoclonal anti-HSP90 (BD Transduction Laboratories, 610419), and rabbit polyclonal anti-GFP (Thermo Fisher Scientific, A6455) antibodies. The secondary antibodies used were HRP-conjugated goat polyclonal anti-rabbit IgG (Jackson ImmunoResearch Laboratories, 111-035-144) and HRP-conjugated goat polyclonal anti-mouse IgG (Jackson ImmunoResearch Laboratories, 115-035-003) antibodies. To induce mitophagy, HeLa cells were treated with 10 μM carbonyl cyanide *m*-chlorophenyl hydrazine (CCCP; Sigma-Aldrich) for 45 min, or 10 μM oligomycin (Cabiochem, 495455-10MGCN) and 4 μM antimycin A (Sigma-Aldrich, A8674) for 18 h. After cells had been treated with oligomycin and antimycin A for >6 h, 10 μM Q-VD-OPH (SM Biochemicals, SMPH001) was added to block apoptotic cell death. To inhibit the formation of isolation membranes in the 1,6-hexanediol (Sigma-Aldrich, 240117-50G) treatment experiment, 20 μM wortmannin (Sigma-Aldrich, W1628-1MG) was added into the medium.

Immunoprecipitation and immunoblotting

Cell lysates were prepared in a lysis buffer (50 mM Tris-HCl pH 7.4, 150 mM NaCl, 1 mM EDTA, 1% Triton X-100, EDTA-free protease inhibitor cocktail [19543200; Roche]). After centrifugation at 17,700 × *g* for 10 min, the supernatants were subjected to immunoprecipitation using anti-FLAG M2 magnetic beads (M8823-1ML; Sigma-Aldrich). Precipitated immunocomplexes were washed three times with

lysis buffer and boiled in sample buffer (46.7 mM Tris-HCl, pH 6.8, 5% glycerol, 1.67% sodium dodecyl sulfate, 1.55% dithiothreitol, and 0.02% bromophenol blue). For immunoprecipitation of ATG9 vesicles, cells were disrupted by Dounce homogenization with hypotonic lysis buffer (10 mM HEPES, pH 7.9, 1.5 mM $MgCl_2$ and 10 mM KCl, EDTA-free protease inhibitor cocktail [19543200; Roche]). Disruption was carried out by applying 35 strokes while the cell suspension was cooled on ice. The supernatants were subjected to immunoprecipitation using anti-FLAG M2 magnetic beads (M8823-1ML; Sigma-Aldrich). For immunoblotting, the samples were separated by SDS-PAGE and transferred to Immobilon-P polyvinylidene difluoride membranes (Millipore, WBKLS0500) with the Trans-Blot Turbo Transfer System (Bio-Rad). After incubation with the relevant antibody in 5% skim milk in 20 mM Tris-HCl, 150 mM NaCl, and 0.1% Tween 20 (02194841-CF; MP Biomedicals), the signals from incubation with SuperSignal West Pico Chemiluminescent Substrate (Thermo Fisher Scientific, 34579) were detected with the FUSION SOLO.7S.EDGE imaging system (Vilber-Lourmat). Contrast and brightness adjustment and quantification were performed using the image processing software Fiji[64].

Fluorescence recovery after photobleaching

In-cell fluorescence recovery after photobleaching (FRAP) analyses were performed with an Olympus Fluoview FV3000 confocal microscope equipped with a 60× oil-immersion objective lens (1.40 NA, Olympus). The chamber was maintained at 37°C

and continuously supplied with humidified 5% CO_2. Bleaching was performed using 80% laser power (488 or 561 nm laser), and images were captured every 5 s for 30 frames. Recovery curves and fitting were analyzed using OriginPro 2022. The fluorescence intensity of the bleached spot, an unbleached control spot, and the background was measured using the software package Fiji. Background intensity was subtracted, and the intensity values of the region of interest are reported relative to the pre-bleached images during image acquisition. Each data point represents the mean and standard error of fluorescence intensities in more than three unbleached (control) or bleached (experimental) spots.

Live-cell imaging

Living imaging was conducted with the Olympus SpinSR10 spinning-disk confocal super-resolution microscope equipped with a Hamamatsu ORCA-Flash 4.0 camera, a UPLAPO OHR 100 × (NA 1.50) lens, and the SORA disk in place. The microscope was operated with Olympus cellSens Dimension 2.3 software. Cells were passaged onto a four-chamber glass-bottom dish (Greiner Bio-One) for more than 24 h before imaging. To induce mitophagy, cells were incubated with 10 μM CCCP in the presence of 200 nM SF650-conjugated Halo ligand (GoryoChemical, A308-02). During observation, cells were kept in an incubator (Tokai Hit) supplied with 5% CO_2 at 37°C. Images were processed using the image processing software package Fiji[64]. Fluorescence intensity of indicated fluorophores was measured by Fiji, and spline connected graphs were created using OriginPro 2022 software.

Immunofluorescence imaging

Cells were fixed with 4% PFA in 0.1 M phosphate buffer (pH 7.3) for 15 min at room temperature (RT) and washed with PBS. Fixed cells were incubated with 10 μg/mL digitonin for 5 min at RT and washed with PBS. Then, cells were incubated with primary antibodies diluted (1:1000) in blocking buffer (3% BSA, in PBS) for 1 h at RT, washed with PBS, incubated with Alexa Fluor-conjugated secondary antibodies (1:1000) in blocking buffer for 60 min at RT, washed again, and mounted on coverslips. Colocalization was calculated by Fiji plugins BIOP JACoP, with the threshold of the ATG9A channel fixed to 500. ATG9A-positive areas out of GFP-positive areas were calculated to obtain the overlapping areas.

Results

Autophagy adaptors show distinct distributions during Parkin-mediated mitophagy

To better understand the behaviors of each autophagy adaptor, I analyzed their localization during Parkin-mediated mitophagy in HeLa cells. Wild-type HeLa cells lack endogenous Parkin, thus I generated the HeLa cell line that stably expresses HA-Parkin. I overexpressed GFP-tagged autophagy adaptors p62, OPTN, NBR1, NDP52, and TAX1BP1 and imaged their localization at 45 ~60 min after the mitochondrial uncoupler carbonyl cyanide *m*-chlorophenylhydrazone (CCCP) incubation. When mitophagy was induced by treatment with CCCP in HeLa cells expressing exogenous Parkin, the autophagy adaptors p62, OPTN, NBR1, NDP52, and TAX1BP1 translocated to mitochondria, as previously observed (Fig. 4)[52, 65-68]. Ubiquitin and all of these autophagy adaptors were distributed evenly on the surface of separate mitochondria (Mt; Fig. 4). In contrast, these adaptors exhibited distinct localization patterns during the formation of isolation membranes on mitochondria (Mt–IM; Fig. 5A). The signals of OPTN and NDP52 were enriched in areas where LC3B signals, an isolation membrane marker, colocalized, while they were mostly absent from the LC3B-negative side of the same mitochondria (Fig. 5A and B). However, this inhomogeneous distribution pattern was not observed for ubiquitin, p62, NBR1, and TAX1BP1 (Fig. 5A and B). Unlike OPTN and NDP52, p62 showed enrichment between clustered mitochondria (Mt-Mt), which is consistent with previous reports

(Fig. 6A and B)[66]. Also, Endogenous OPTN and NDP52 also showed clear enrichment on the LC3B-positive areas in comparison to the LC3B-negative side, confirming that this localization is not caused by the overexpression of adaptors (Fig. 7). These accumulation patterns cannot be explained by the stoichiometric interaction of the autophagy adaptors with ubiquitinated proteins that are evenly distributed on mitochondria.

The localization of autophagy adaptors may be affected by their interaction with other adaptors[69, 70]. To examine the localization of each adaptor on its own, I used HeLa cells lacking all five autophagy adaptors (penta KO cells) and re-expressed adaptors separately to exclude the effect of other adaptors[18]. In penta KO cells, OPTN and NDP52 exhibited significant enrichment in LC3B-positive areas, similar to that observed in wild-type cells, suggesting that this accumulation occurred independently of heterologous interaction with other adaptors (Fig. 8A and B). Mitophagy was not restored by exogenous expression of p62 or NBR1 in penta KO cells, and thus colocalization with LC3 could not be tested for these two adaptors[18]. The accumulation of p62 between clustered mitochondria was also observed in penta KO cells (Fig. 9A and B). Given the uniform distribution of ubiquitinated proteins on mitochondrial surfaces, these data suggest that autophagy adaptors exhibit non-stoichiometric enrichment between membranes. Hereafter, I used penta KO cells to study each autophagy adapter individually.

OPTN and NDP52 show a dynamic exchange between the mitochondrial surface and cytosol

I hypothesized that the non-stoichiometric distribution of the autophagy adaptors on ubiquitinated mitochondria could be explained by LLPS because liquid-like condensates always show higher protein concentrations. Also, typical condensates generated by LLPS exhibit rapid exchange of their components, which is often demonstrated by fluorescence recovery after photobleaching (FRAP) analysis[71, 72]. I first conducted FRAP experiments for separate (i.e., unclustered) mitochondria in CCCP-treated cells. As expected, ubiquitin showed virtually no recovery because it was conjugated to mitochondrial membrane proteins (Fig. 10A and B). Additionally, p62 recovered only slightly, suggesting a minute exchange between the mitochondrial surface and cytosol (Fig. 10A and B). In contrast, OPTN and NDP52 showed a rapid recovery, indicating a dynamic exchange of these adaptors between the mitochondrial surface and the cytosol (Fig. 10A and B).

Next, I examined the dynamics of adaptors between mitochondria and isolation membranes. OPTN and NDP52 showed partial recovery (Fig. 11A and B). Although this result indicates some exchange of these adaptors between membranes, the incomplete recovery suggests the existence of a gel-like or immobile fraction. Treatment with 1,6-hexanediol, which can be used to dissolve condensates, dispersed OPTN from mitochondria without isolation membranes, suggesting that OPTN accumulation is supported by weak interactions (Fig. 12). These results indicate that OPTN and NDP52 on ubiquitinated mitochondria are mobile and can quickly exchange between the mitochondrial surface and the cytosol, supporting the hypothesis that they form phase-separated condensates on damaged mitochondria.

OPTN condensates redistribute upon membrane contact

Coalescence is considered as one of the properties of phase-separated droplets. If autophagy adaptors form condensates on the mitochondria, what will happen when mitochondria contact. To unravel this question, I observed cells by using live-cell imaging. When two small mitochondria with uniform OPTN distributions on their surface approached each other, OPTN redistributed and formed a smooth surface that covered the two adjacent mitochondria (Fig. 13A and 14A). Notably, strong OPTN enrichment was observed in the cleft between the two mitochondria (arrowheads, Fig. 13A and 14A), showing a pattern distinct from that of the outer membrane protein Omp25 (OPTN signal peaks localized outside of Omp25 signal peaks) (Fig. 13B and 14B). This phenomenon was apparent when the size of both (Fig. 13A) or one (Fig. 14A) of the two mitochondria was less than 1 μm. Although OPTN formed sheet-like rather than spherical condensates, this phenomenon appeared to be similar to condensate coalescence, which is one of the hallmarks of liquid-like condensates[41]. Furthermore, when an isolation membrane started to engulf a mitochondrion, OPTN, which was initially distributed uniformly on the mitochondrial surface, underwent redistribution to the area contacting the isolation membrane (Fig. 15A). OPTN signals on the isolation membrane-negative side of the mitochondrion diminished during this process (Fig. 15A and B). The OPTN-enriched region expanded together with the isolation membrane thereafter (Fig. 15A). Taken together, our experimental data support the hypothesis that OPTN forms sheet-like phase-separated condensates on the surface of ubiquitinated mitochondria, exhibiting liquid-like properties.

Liquid-like property of OPTN condensates is required for mitophagy

To investigate the importance of the liquid-like nature of OPTN condensates on mitochondria, I sought to reduce its liquidity by strengthening the interaction but reducing the multivalency between ubiquitin and GFP–OPTN constructs. To achieve this, I utilized the anti-green fluorescent protein (GFP) nanobody, which exhibits a high binding affinity to GFP[73]. Fusing the anti-GFP nanobody to the N-terminus of ubiquitin (nanobody–mRuby–Ub) (Fig. 17A, bottom panel) resulted in significantly enhanced binding to GFP–OPTN (Fig. 16). Deleting the ubiquitin-binding domain in ABINs and NEMO (UBAN domain) from OPTN (GFP–OPTNΔUBAN) eliminated the interaction with ubiquitinated proteins (Fig. 17A). Wild-type GFP–OPTN accumulated on ubiquitinated mitochondria, but GFP–OPTNΔUBAN failed to do so (Fig. 17A, top and middle panels). In contrast, the expression of nanobody–mRuby–Ub rescued the recruitment of GFP–OPTNΔUBAN to mitochondria (Fig. 17A, lower panel). FRAP experiments revealed that, compared with wild-type GFP–OPTN (with mRuby–Ub, not nanobody-mRuby–Ub), GFP–OPTNΔUBAN showed a substantial decrease in recovery on mitochondria when co-expressed with nanobody–mRuby–Ub, indicating a reduction in its dynamic properties (Fig. 17B).

I then evaluated the effect of impaired OPTN liquidity on mitophagy using the recently developed HaloTag cleavage assay[74]. This assay utilizes the ligand-dependent conformational change of HaloTag (Halo); ligand-free Halo is efficiently degraded in lysosomes, whereas ligand-bound Halo becomes resistant to lysosomal degradation. When Halo is expressed in the mitochondrial matrix by fusing to the

mitochondrial presequence of Fo-ATPase subunit 9 and SNAP-tag (mtHalo–SNAP), I can measure the extent of mitochondrial degradation by quantifying the amount of processed free Halo out of the total amount of Halo (mtHalo–SNAP + processed Halo). Mitophagy activity, which was impaired in penta KO cells, was restored by the expression of GFP–OPTN (Fig. 18A and B). However, GFP–OPTNΔUBAN failed to restore mitophagy, even when it was co-expressed with nanobody–mRuby–Ub to rescue ubiquitin binding and mitochondrial localization (Fig. 17A, 18A and B). These data suggest that the localization of OPTN on mitochondria and its binding to ubiquitin alone is insufficient for mitophagy, and the liquidity of OPTN is important for effective mitophagy.

Liquid-like property of OPTN condensates is required for the recruitment of ATG9 vesicles

ATG9 vesicles are considered to be one of the sources of autophagosomal membranes[75]. Upon mitophagy induction, ATG9 vesicles accumulate at the sites of autophagosome formation[76]. OPTN plays a crucial role in this process by recruiting ATG9 vesicles to induce mitophagy[35]. In general, liquid-like condensates can be involved in clustering small vesicles such as synaptic vesicles, which exemplify complete wetting[77, 78]. Indeed, ATG9 vesicles are incorporated into condensates containing a glaucoma-associated OPTN mutant[79] and synapsin[80]. I, therefore, hypothesized that the liquid-like properties of OPTN condensates on mitochondria facilitate the recruitment of ATG9 vesicles. Without CCCP, ATG9 was disperse in cytosol (Fig. 19A), no matter GFP–OPTN or GFP–OPTNΔUBAN. Consistent with previous reports[35, 76], ATG9A was recruited to depolarized mitochondria in cells expressing GFP–OPTN (Fig. 19B). However, this ATG9A recruitment was almost completely abolished in cells expressing nanobody–mRuby–Ub and GFP–OPTNΔUBAN (Fig. 19B and C), even though GFP–OPTNΔUBAN still retains the ATG9A-interacting domain and the ability to bind with the ATG9 vesicles (Fig. 20A and B). Taken together, these findings suggest that the liquidity of sheet-like OPTN condensates on the mitochondrial surface is crucial for recruiting ATG9 vesicles and executing mitophagy.

Discussion

LLPS by autophagy adaptors during Parkin-mediated mitophagy

During Parkin-mediated mitophagy pathway, autophagy adaptors bridge ubiquitinated mitochondrial and isolation membranes by UBD and LIR motif. In the present study, I discovered that autophagy adaptors show distinct distributions in different mitochondrial morphology. Some adaptors accumulate on ubiquitinated mitochondria with non-stoichiometric distribution compared with ubiquitin signals. They displayed characteristics consistent with phase-separated structures, including dynamic exchange with cytosol and redistribution upon coalescence. Notably, I observed the enrichment of OPTN at the isolation membrane-positive region, which expanded along with the elongation of the isolation membrane. These findings suggest that phase-separated adaptors facilitate the effective engulfment of mitochondria by the isolation membrane through the wetting effect and capillary forces (Fig. 21, right panel). Moreover, the liquidity of OPTN condensates is critical for the localization of ATG9 vesicles onto ubiquitinated mitochondria, indicating that partial or complete wetting of phase-separated adaptors to ATG9 vesicles may be crucial for their recruitment to and/or retention on mitochondria (Fig. 21, left panel). Therefore, I propose that LLPS of autophagy adaptors plays a critical role in two distinct steps of mitophagy by producing capillary forces, first, at the initiation step by recruiting and retaining the ATG9 vesicles in the condensates and, second, at the autophagosome elongation step by facilitating the attachment between ubiquitinated mitochondria and

the isolation membrane.

LLPS in bulk and selective autophagy

Recent reports have shed light on the importance of LLPS in selective autophagy[46]. In lysophagy, p62 undergoes LLPS on lysosomes to facilitate efficient lysophagy together with HSP27, which maintains the liquidity of p62 and prevents its gelation[52]. This may also be mediated by the wetting between damaged lysosomes and the isolation membrane by phase-separated p62. Indeed, p62 itself forms phase-separated condensates along with ubiquitinated proteins, producing capillary forces by the wetting effect to facilitate the engulfment by the isolation membrane[51]. Similarly, in the yeast cytosol-to-vacuole targeting (Cvt) pathway, the cargo protein Ape1 forms gel-like condensates with Atg19 on the surface of Ape1 condensates, enabling their sequestration by the isolation membrane [81]. The liquid-like property is vital for the cargo transportation by the Cvt pathway. For instance, the loss of liquidity caused by a Pro-to-Leu mutation at residue 22 (P22L) in the Ape1 propeptide results in imparired Cvt pathway function, as it leads to the formation of amorphous, immobile condensates. Importantly, this mutation neither impairs the formation of Ape1 condensates nor severely reduces the interaction with Atg19 [81]. These examples together with our observations highlight the importance of LLPS and the wetting phenomena in various selective autophagy processes.

LLPS may also be important for non-selective bulk autophagy. In yeast, the Atg1 complex (the ULK1 complex in mammals) forms pre-autophagosomal structures

(PASs), which have been shown to be condensates driven by LLPS[82]. Phase separation in this context provides a high local concentration of the Atg1 complex to support the autoactivation of Atg1 kinase[83]. Mammalian autophagy factors also accumulate at the autophagosome formation site; FIP200, a subunit of the autophagy-initiation complex, undergoes LLPS triggered by calcium transients[84]. The liquid-like nature of these autophagy-initiating structures may also be important for the recruitment of Atg9/ATG9 vesicles through the wetting effect.

The importance of phase separation during mitophagy

In contrast to Parkin-mediated mitophagy, hypoxia-induced mitophagy does not involve autophagy adaptors, and instead, the outer mitochondrial membrane proteins NIX (also known as BNIP3L) and BNIP3 directly interact with ATG8 homologs on the isolation membrane[14, 20]. In this context, ATG8 proteins interact with NIX or BNIP3, likely in a one-to-one manner.

This raises the problem of why phase separation of autophagy adaptors is essential for Parkin-mediated mitophagy. One possibility is that the quick induction and execution of Parkin-mediated mitophagy requires amplification of the reactions through increased local concentration of adaptors and autophagy-related proteins facilitated by LLPS. This is consistent with the fact that mitophagy-inducing signals are also amplified by a mechanism involving phosphorylated ubiquitin[85-87]. Alternatively, Parkin-mediated mitophagy requires a high level of precision and selectivity; mitophagy should be induced only for damaged mitochondria, which is

ensured by the recruitment and retention of ATG9 vesicles only on phase-separated adaptor-positive mitochondria. This strict specificity would enable proper quality control of the mitochondria.

While our study provides valuable insights into LLPS during mitophagy, it is important to note several limitations. Loss of the C-terminal domain of OPTN, could be considered an extreme modification to the protein. Although this mutant did not affect binding to ATG9A vesicles. It can still cause the structure change of OPTN which may affect the mitophagy activity. Additionally, all the experiments were conducted in cells, limiting the physiological importance of our findings. For example, in the case of Amyotrophic lateral sclerosis (ALS), the accumulation of damaged or malfunctioning mitochondria is considered a factor contributing to the disease. Despite our understanding of the associations of PINK-1/Parkin with Parkinson's disease and OPTN/TBK1 with ALS, the significance of this overlap remains unclear. Furthermore, mutations in OPTN have been identified in ALS patients. However, it is still unclear whether these mutants affect the fluidity of OPTN and consequently impede the clearance of damaged mitochondria through mitophagy.. Future study would be required to elucidate the functions and physiological importance of LLPS by autophagy adaptors in mitophagy and beyond.

References

[1] Y. Chun and J. Kim, "Autophagy: An Essential Degradation Program for Cellular Homeostasis and Life," *Cells,* vol. 7, no. 12, Dec 2018, Art no. 278, doi: 10.3390/cells7120278.

[2] N. Mizushima and B. Levine, "Autophagy in Human Diseases," *New England Journal of Medicine,* vol. 383, no. 16, pp. 1564-1576, Oct 2020, doi: 10.1056/NEJMra2022774.

[3] H. Nakatogawa, "Mechanisms governing autophagosome biogenesis," *Nature Reviews Molecular Cell Biology,* vol. 21, no. 8, pp. 439-458, Aug 2020, doi: 10.1038/s41580-020-0241-0.

[4] Z. P. Xie and D. J. Klionsky, "Autophagosome formation: Core machinery and adaptations," *Nature Cell Biology,* vol. 9, no. 10, pp. 1102-1109, Oct 2007, doi: 10.1038/ncb1007-1102.

[5] K. Suzuki and Y. Ohsumi, "Molecular machinery of autophagosome formation in yeast, Saccharomyces cerevisiae," *Febs Letters,* vol. 581, no. 11, pp. 2156-2161, May 2007, doi: 10.1016/j.febslet.2007.01.096.

[6] N. Mizushima, Y. Ohsumi, and T. Yoshimori, "Autophagosome formation in mammalian cells," *Cell Structure and Function,* vol. 27, no. 6, pp. 421-429, Dec 2002, doi: 10.1247/csf.27.421.

[7] N. Mizushima, "Regulation of autophagosome formation in mammalian cells," *Autophagy,* vol. 5, no. 6, pp. 898-899, Aug 2009.

[8] T. Lamark and T. Johansen, "Mechanisms of Selective Autophagy," *Annual*

Review of Cell and Developmental Biology, Vol 37, vol. 37, pp. 143-169, 2021, doi: 10.1146/annurev-cellbio-120219-035530.

[9] J. N. S. Vargas, M. Hamasaki, T. Kawabata, R. J. Youle, and T. Yoshimori, "The mechanisms and roles of selective autophagy in mammals," *Nat. Rev. Mol. Cell Biol.,* vol. 24, no. 3, pp. 167-185, Mar 2023, doi: 10.1038/s41580-022-00542-2.

[10] B. Bauer, S. Martens, and L. Ferrari, "Aggrephagy at a glance," *Journal of Cell Science,* vol. 136, no. 10, May 2023, Art no. jcs260888, doi: 10.1242/jcs.260888.

[11] H. Chino and N. Mizushima, "ER-Phagy: Quality Control and Turnover of Endoplasmic Reticulum," *Trends in Cell Biology,* vol. 30, no. 5, pp. 384-398, May 2020, doi: 10.1016/j.tcb.2020.02.001.

[12] C. Papadopoulos, B. Kravic, and H. Meyer, "Repair or Lysophagy: Dealing with Damaged Lysosomes," *Journal of Molecular Biology,* vol. 432, no. 1, pp. 231-239, Jan 2020, doi: 10.1016/j.jmb.2019.08.010.

[13] A. Reggio, V. Buonomo, and P. Grumati, "Eating the unknown: Xenophagy and ER-phagy are cytoprotective defenses against pathogens," *Experimental Cell Research,* vol. 396, no. 1, Nov 2020, Art no. 112276, doi: 10.1016/j.yexcr.2020.112276.

[14] M. Onishi, K. Yamano, M. Sato, N. Matsuda, and K. Okamoto, "Molecular mechanisms and physiological functions of mitophagy," *Embo Journal,* vol. 40, no. 3, Feb 2021, Art no. e104705, doi: 10.15252/embj.2020104705.

[15] T. Lamark and T. Johansen, "Aggrephagy: selective disposal of protein aggregates by macroautophagy," *International journal of cell biology,* vol. 2012, 2012.

[16] E. R. Gallagher and E. L. Holzbaur, "The selective autophagy adaptor p62/SQSTM1 forms phase condensates regulated by HSP27 that facilitate the clearance of damaged lysosomes via lysophagy," *Cell Reports,* vol. 42, no. 2, 2023.

[17] V. Sharma, S. Verma, E. Seranova, S. Sarkar, and D. Kumar, "Selective Autophagy and Xenophagy in Infection and Disease," *Frontiers in Cell and Developmental Biology,* vol. 6, Nov 2018, Art no. 147, doi: 10.3389/fcell.2018.00147.

[18] M. Lazarou *et al.*, "The ubiquitin kinase PINK1 recruits autophagy receptors to induce mitophagy," *Nature,* vol. 524, no. 7565, pp. 309-314, Aug 20 2015, doi: 10.1038/nature14893.

[19] H. Chino, T. Hatta, T. Natsume, and N. Mizushima, "Intrinsically Disordered Protein TEX264 Mediates ER-phagy," *Molecular Cell,* vol. 74, no. 5, pp. 909-+, Jun 2019, doi: 10.1016/j.molcel.2019.03.033.

[20] I. Novak *et al.*, "Nix is a selective autophagy receptor for mitochondrial clearance," *EMBO reports,* vol. 11, no. 1, pp. 45-51 %@ 1469-221X, 2010.

[21] M. R. Duchen, "Mitochondria and calcium: from cell signalling to cell death," *Journal of Physiology-London,* vol. 529, no. 1, pp. 57-68, Nov 2000, doi: 10.1111/j.1469-7793.2000.00057.x.

[22] S. A. Susin *et al.*, "Molecular characterization of mitochondrial apoptosis-inducing factor," *Nature,* vol. 397, no. 6718, pp. 441-446, Feb 1999, doi: 10.1038/17135.

[23] M. Calvo-Rodriguez and B. J. Bacskai, "Mitochondria and Calcium in Alzheimer's Disease: From Cell Signaling to Neuronal Cell Death," *Trends in Neurosciences,* vol. 44, no. 2, pp. 136-151, Feb 2021, doi: 10.1016/j.tins.2020.10.004.

[24] V. Brillo, L. Chieregato, L. Leanza, S. Muccioli, and R. Costa, "Mitochondrial Dynamics, ROS, and Cell Signaling: A Blended Overview," *Life-Basel,* vol. 11, no. 4, Apr 2021, Art no. 332, doi: 10.3390/life11040332.

[25] C. Guo, L. Sun, X. Chen, and D. Zhang, "Oxidative stress, mitochondrial damage and neurodegenerative diseases," *Neural regeneration research,* vol. 8, no. 21, p. 2003, 2013.

[26] B. Van Houten, V. Woshner, and J. H. Santos, "Role of mitochondrial DNA in toxic responses to oxidative stress," *DNA repair,* vol. 5, no. 2, pp. 145-152 %@ 1568-7864, 2006.

[27] S. B. Hollensworth, C.-C. Shen, J. E. Sim, D. R. Spitz, G. L. Wilson, and S. P. LeDoux, "Glial cell type-specific responses to menadione-induced oxidative stress," *Free Radical Biology and Medicine,* vol. 28, no. 8, pp. 1161-1174 %@ 0891-5849, 2000.

[28] L. Uoselis, T. N. Nguyen, and M. Lazarou, "Mitochondrial degradation: Mitophagy and beyond," *Molecular Cell %@ 1097-2765,* 2023.

[29] I. G. Ganley and A. Simonsen, "Diversity of mitophagy pathways at a glance," *Journal of Cell Science,* vol. 135, no. 23, Dec 2022, Art no. jcs259748, doi: 10.1242/jcs.259748.

[30] T. Wauer, M. Simicek, A. Schubert, and D. Komander, "Mechanism of phospho-ubiquitin-induced PARKIN activation," *Nature,* vol. 524, no. 7565, pp. 370-+, Aug 2015, doi: 10.1038/nature14879.

[31] J. W. Harper, A. Ordureau, and J. M. Heo, "Building and decoding ubiquitin chains for mitophagy," *Nature Reviews Molecular Cell Biology,* vol. 19, no. 2, pp. 93-108, Feb 2018, doi: 10.1038/nrm.2017.129.

[32] N. C. Chan *et al.*, "Broad activation of the ubiquitin-proteasome system by Parkin is critical for mitophagy," *Human Molecular Genetics,* vol. 20, no. 9, pp. 1726-1737, May 2011, doi: 10.1093/hmg/ddr048.

[33] M. Lazarou *et al.*, "The ubiquitin kinase PINK1 recruits autophagy receptors to induce mitophagy," *Nature,* vol. 524, no. 7565, pp. 309-+, Aug 2015, doi: 10.1038/nature14893.

[34] K. Okatsu *et al.*, "p62/SQSTM1 cooperates with Parkin for perinuclear clustering of depolarized mitochondria," *Genes to Cells,* vol. 15, no. 8, pp. 887-900, Aug 2010, doi: 10.1111/j.1365-2443.2010.01426.x.

[35] K. Yamano *et al.*, "Critical role of mitochondrial ubiquitination and the OPTN-ATG9A axis in mitophagy," *Journal of Cell Biology,* vol. 219, no. 9, Sep 2020, Art no. e201912144, doi: 10.1083/jcb.201912144.

[36] A. Musacchio, "On the role of phase separation in the biogenesis of

membraneless compartments," *Embo Journal,* vol. 41, no. 5, Mar 2022, Art no. e109952, doi: 10.15252/embj.2021109952.

[37] T. Hirose, K. Ninomiya, S. Nakagawa, and T. Yamazaki, "A guide to membraneless organelles and their various roles in gene regulation," *Nat. Rev. Mol. Cell Biol.,* vol. 24, no. 4, pp. 288-304, Apr 2023, doi: 10.1038/s41580-022-00558-8.

[38] C. P. Brangwynne *et al.*, "Germline P Granules Are Liquid Droplets That Localize by Controlled Dissolution/Condensation," *Science,* vol. 324, no. 5935, pp. 1729-1732, Jun 2009, doi: 10.1126/science.1172046.

[39] S. F. Banani, H. O. Lee, A. A. Hyman, and M. K. Rosen, "Biomolecular condensates: organizers of cellular biochemistry," *Nature Reviews Molecular Cell Biology,* vol. 18, no. 5, pp. 285-298, May 2017, doi: 10.1038/nrm.2017.7.

[40] B. Wang, L. Zhang, T. Dai, Z. R. Qin, H. S. Lu, and F. F. Zhou, "Liquid-liquid phase separation in human health and diseases," *Signal Transduction and Targeted Therapy,* vol. 6, no. 1, Aug 2021, Art no. 290, doi: 10.1038/s41392-021-00678-1.

[41] A. A. Hyman, C. A. Weber, and F. Juelicher, "Liquid-Liquid Phase Separation in Biology," *Annual Review of Cell and Developmental Biology, Vol 30,* vol. 30, pp. 39-58, 2014, doi: 10.1146/annurev-cellbio-100913-013325.

[42] P. A. Chong and J. D. Forman-Kay, "Liquid-liquid phase separation in cellular signaling systems," *Current Opinion in Structural Biology,* vol. 41, pp. 180-186, Dec 2016, doi: 10.1016/j.sbi.2016.08.001.

[43] T. J. Nott *et al.*, "Phase Transition of a Disordered Nuage Protein Generates Environmentally Responsive Membraneless Organelles," *Molecular Cell,* vol. 57, no. 5, pp. 936-947, Mar 2015, doi: 10.1016/j.molcel.2015.01.013.

[44] L. P. Bergeron-Sandoval, N. Safaee, and S. W. Michnick, "Mechanisms and Consequences of Macromolecular Phase Separation," *Cell,* vol. 165, no. 5, pp. 1067-1079, May 2016, doi: 10.1016/j.cell.2016.05.026.

[45] Y. Shin and C. P. Brangwynne, "Liquid phase condensation in cell physiology and disease," *Science,* vol. 357, no. 6357, Sep 2017, Art no. eaaf4382, doi: 10.1126/science.aaf4382.

[46] N. N. Noda, Z. Wang, and H. Zhang, "Liquid-liquid phase separation in autophagy," *Journal of Cell Biology,* vol. 219, no. 8, Aug 2020, Art no. e202004062, doi: 10.1083/jcb.202004062.

[47] X. Ma, P. Li, and L. Ge, "Targeting of biomolecular condensates to the autophagy pathway," *Trends in Cell Biology,* vol. 33, no. 6, pp. 505-516, 2023.

[48] G. Zaffagnini *et al.*, "p62 filaments capture and present ubiquitinated cargos for autophagy," *EMBO J,* vol. 37, no. 5, Mar 1 2018, doi: 10.15252/embj.201798308.

[49] D. Sun, R. Wu, J. Zheng, P. Li, and L. Yu, "Poly-ubiquitin chain-induced p62 phase separation drives autophagic cargo segregation," *Cell Res,* vol. 28, no. 4, pp. 405-415, Apr 2018, doi: 10.1038/s41422-018-0017-7.

[50] D. X. Sun, R. B. Wu, J. X. Zheng, P. L. Li, and L. Yu, "Poly-ubiquitin chain-induced p62 phase separation drives autophagic cargo segregation," *Cell*

Research, vol. 28, no. 4, pp. 405-415, Apr 2018, doi: 10.1038/s41422-018-0017-7.

[51] J. Agudo-Canalejo *et al.*, "Wetting regulates autophagy of phase-separated compartments and the cytosol," *Nature,* vol. 591, no. 7848, pp. 142-+, Mar 2021, doi: 10.1038/s41586-020-2992-3.

[52] E. R. Gallagher and E. L. F. Holzbaur, "The selective autophagy adaptor p62/SQSTM1 forms phase condensates regulated by HSP27 that facilitate the clearance of damaged lysosomes via lysophagy," *Cell Reports,* vol. 42, no. 2, 2023.

[53] S. Z. Peng *et al.*, "Phase separation of Nur77 mediates celastrol-induced mitophagy by promoting the liquidity of p62/SQSTM1 condensates," *Nature Communications,* vol. 12, no. 1, Oct 2021, Art no. 5989, doi: 10.1038/s41467-021-26295-8.

[54] H. Kusumaatmaja, A. I. May, and R. L. Knorr, "Intracellular wetting mediates contacts between liquid compartments and membrane-bound organelles," *Journal of Cell Biology,* vol. 220, no. 10, Oct 2021, Art no. e202103175, doi: 10.1083/jcb.202103175.

[55] B. Gouveia, Y. Kim, J. W. Shaevitz, S. Petry, H. A. Stone, and C. P. Brangwynne, "Capillary forces generated by biomolecular condensates," *Nature,* vol. 609, no. 7926, pp. 255-264, Sep 2022, doi: 10.1038/s41586-022-05138-6.

[56] H. Kusumaatmaja *et al.*, "Wetting of phase-separated droplets on plant vacuole

membranes leads to a competition between tonoplast budding and nanotube formation," *Proceedings of the National Academy of Sciences of the United States of America,* vol. 118, no. 36, Sep 2021, Art no. e2024109118, doi: 10.1073/pnas.2024109118.

[57] R. W. Style, A. Jagota, C.-Y. Hui, and E. R. J. A. R. o. C. M. P. Dufresne, "Elastocapillarity: Surface tension and the mechanics of soft solids," vol. 8, pp. 99-118, 2017.

[58] J. S. Wexler, T. M. Heard, and H. A. J. P. r. l. Stone, "Capillary bridges between soft substrates," vol. 112, no. 6, p. 066102, 2014.

[59] T. Saitoh, H. Nakano, N. Yamamoto, and S. J. F. l. Yamaoka, "Lymphotoxin-β receptor mediates NEMO-independent NF-κB activation," vol. 532, no. 1-2, pp. 45-51, 2002.

[60] T. Kitamura *et al.*, "Retrovirus-mediated gene transfer and expression cloning: Powerful tools in functional genornics," *Experimental Hematology,* vol. 31, no. 11, pp. 1007-1014, Nov 2003, doi: 10.1016/j.exphem.2003.07.005.

[61] D. J. Scott *et al.*, "A Novel Ultra-Stable, Monomeric Green Fluorescent Protein For Direct Volumetric Imaging of Whole Organs Using CLARITY," *Scientific reports,* vol. 8, no. 1, p. 667, 2018/01/12 2018, doi: 10.1038/s41598-017-18045-y.

[62] B. T. Bajar *et al.*, "Improving brightness and photostability of green and red fluorescent proteins for live cell imaging and FRET reporting," *Scientific reports,* vol. 6, no. 1, p. 20889, 2016.

[63] Y. Eura, N. Ishihara, S. Yokota, and K. J. T. J. o. B. Mihara, "Two mitofusin proteins, mammalian homologues of FZO, with distinct functions are both required for mitochondrial fusion," vol. 134, no. 3, pp. 333-344, 2003.

[64] J. Schindelin *et al.*, "Fiji: an open-source platform for biological-image analysis," *Nature Methods,* vol. 9, no. 7, pp. 676-682, Jul 2012, doi: 10.1038/nmeth.2019.

[65] S. Geisler *et al.*, "PINK1/Parkin-mediated mitophagy is dependent on VDAC1 and p62/SQSTM1," *Nature Cell Biology,* vol. 12, no. 2, pp. 119-U70, Feb 2010, doi: 10.1038/ncb2012.

[66] Y. C. Wong and E. L. Holzbaur, "Optineurin is an autophagy receptor for damaged mitochondria in parkin-mediated mitophagy that is disrupted by an ALS-linked mutation," *Proc Natl Acad Sci U S A,* vol. 111, no. 42, pp. E4439-48, Oct 21 2014, doi: 10.1073/pnas.1405752111.

[67] J. M. Heo, A. Ordureau, J. A. Paulo, J. Rinehart, and J. W. Harper, "The PINK1-PARKIN Mitochondrial Ubiquitylation Pathway Drives a Program of OPTN/NDP52 Recruitment and TBK1 Activation to Promote Mitophagy," *Molecular Cell,* vol. 60, no. 1, pp. 7-20, Oct 2015, doi: 10.1016/j.molcel.2015.08.016.

[68] A. S. Moore and E. L. F. Holzbaur, "Dynamic recruitment and activation of ALS-associated TBK1 with its target optineurin are required for efficient mitophagy," *Proceedings of the National Academy of Sciences of the United States of America,* vol. 113, no. 24, pp. E3349-E3358, Jun 2016, doi:

10.1073/pnas.1523810113.

[69] E. Turco *et al.*, "Reconstitution defines the roles of p62, NBR1 and TAX1BP1 in ubiquitin condensate formation and autophagy initiation," *Nature Communications,* vol. 12, no. 1, Sep 2021, Art no. 5212, doi: 10.1038/s41467-021-25572-w.

[70] A. Gubas and I. Dikic, "A guide to the regulation of selective autophagy receptors," *The FEBS journal,* vol. 289, no. 1, pp. 75-89 %@ 1742-464X, 2022.

[71] N. O. Taylor, M.-T. Wei, H. A. Stone, and C. P. Brangwynne, "Quantifying dynamics in phase-separated condensates using fluorescence recovery after photobleaching," *Biophysical journal,* vol. 117, no. 7, pp. 1285-1300 %@ 0006-3495, 2019.

[72] D. T. McSwiggen, M. Mir, X. Darzacq, and R. Tjian, "Evaluating phase separation in live cells: diagnosis, caveats, and functional consequences," *Genes Dev,* vol. 33, no. 23-24, pp. 1619-1634, Dec 1 2019, doi: 10.1101/gad.331520.119.

[73] U. Rothbauer, K. Zolghadr, S. Muyldermans, A. Schepers, M. C. Cardoso, and H. Leonhardt, "A versatile nanotrap for biochemical and functional studies with fluorescent fusion proteins," *Molecular & Cellular Proteomics,* vol. 7, no. 2, pp. 282-289, Feb 2008, doi: 10.1074/mcp.M700342-MCP200.

[74] W. W. Y. Yim, H. Yamamoto, and N. Mizushima, "A pulse-chasable reporter processing assay for mammalian autophagic flux with HaloTag," *Elife,* vol. 11,

Aug 2022, Art no. e78923, doi: 10.7554/eLife.78923.

[75] H. Yamamoto *et al.*, "Atg9 vesicles are an important membrane source during early steps of autophagosome formation," *Journal of Cell Biology,* vol. 198, no. 2, pp. 219-233, Jul 2012, doi: 10.1083/jcb.201202061.

[76] E. Itakura, C. Kishi-Itakura, I. Koyama-Honda, and N. Mizushima, "Structures containing Atg9A and the ULK1 complex independently target depolarized mitochondria at initial stages of Parkin-mediated mitophagy," *Journal of Cell Science,* vol. 125, no. 6, pp. 1488-1499, Mar 2012, doi: 10.1242/jcs.094110.

[77] D. Milovanovic and P. De Camilli, "Synaptic Vesicle Clusters at Synapses: A Distinct Liquid Phase?," *Neuron,* vol. 93, no. 5, pp. 995-1002, Mar 2017, doi: 10.1016/j.neuron.2017.02.013.

[78] R. Sansevrino, C. Hoffmann, and D. Milovanovic, "Condensate biology of synaptic vesicle clusters," *Trends in Neurosciences,* vol. 46, no. 4, pp. 293-306, Apr 2023, doi: 10.1016/j.tins.2023.01.001.

[79] T. O'Loughlin *et al.*, "OPTN recruitment to a Golgi-proximal compartment regulates immune signalling and cytokine secretion," *Journal of Cell Science,* vol. 133, no. 12, Jun 2020, Art no. jcs239822, doi: 10.1242/jcs.239822.

[80] D. Park, Y. Wu, X. Wang, S. Gowrishankar, A. Baublis, and P. De Camilli, "Synaptic vesicle proteins and ATG9A self-organize in distinct vesicle phases within synapsin condensates," *Nature Communications,* vol. 14, no. 1, p. 455, 2023/01/28 2023, doi: 10.1038/s41467-023-36081-3.

[81] A. Yamasaki *et al.*, "Liquidity Is a Critical Determinant for Selective

Autophagy of Protein Condensates," *Molecular Cell,* vol. 77, no. 6, pp. 1163-+, Mar 2020, doi: 10.1016/j.molcel.2019.12.026.

[82] Y. Fujioka *et al.*, "Phase separation organizes the site of autophagosome formation," *Nature,* vol. 578, no. 7794, pp. 301-305 %@ 0028-0836, 2020.

[83] H. Yamamoto *et al.*, "The intrinsically disordered protein Atg13 mediates supramolecular assembly of autophagy initiation complexes," *Developmental cell,* vol. 38, no. 1, pp. 86-99 %@ 1534-5807, 2016.

[84] Q. Zheng *et al.*, "Calcium transients on the ER surface trigger liquid-liquid phase separation of FIP200 to specify autophagosome initiation sites," *Cell,* vol. 185, no. 22, pp. 4082-4098. e22 %@ 0092-8674, 2022.

[85] L. A. Kane *et al.*, "PINK1 phosphorylates ubiquitin to activate Parkin E3 ubiquitin ligase activity," *Journal of Cell Biology,* vol. 205, no. 2, pp. 143-153, Apr 2014, doi: 10.1083/jcb.201402104.

[86] A. Kazlauskaite *et al.*, "Parkin is activated by PINK1-dependent phosphorylation of ubiquitin at Ser65," *Biochemical Journal,* vol. 460, no. 1, pp. 127-141 %@ 0264-6021, 2014.

[87] F. Koyano *et al.*, "Ubiquitin is phosphorylated by PINK1 to activate parkin," *Nature,* vol. 510, no. 7503, pp. 162-166 %@ 0028-0836, 2014.

Table

Table 1. Primer list for plasmid construction.

Plasmid	Primer sequence (5'->3')	Description
1. pMRX-IHU-mRuby-nano-ubiquitin	aggctcgGGATCCggGAATTCgGCGCAGGTTCAGCTGGTTGAAAGCGGTG	amplify GFP-nanobody
	gctgCCgcttccgctaccTTTGCTGCTAACGGTAACCTGGGTGCCCTGAC	
	ggtagcggaagcGGcagcCAGATTTTCGTGAAAACCCTTACGGGGAAGAC	amplify ubiquitin
	gtaGCGGCCGCtCTCGAGaccTTAACCACCACGAAGTCTCAACACAAG	
2. pMRX-IPU-GFP-OPTNΔUBAN	CCAAACAGCTGCAAATGAATGATGCTTTCGAAGACGGAGGCAGGC	OPTN site mutant
	CTTCGAAAGCATCATTCATTTGCAGCTGTTTGGAAGCCAGAGCCTTC	
3. pMRX-IPU-muGFP-(MCS)	ccggatctgccATCGATataAAGCTTgccaccATGGTGAGCAAGGGCGAGGAGCTG	A206K EGFP point mutant
	GCtTTACTCGAGacccGAATTCccGGATCCcgagcctgaaccCTTGTACAGCTCGTCCATGCCatgAGTG	
4. pMRX-IPU-muGFP-Ubiquitin	ggttcaggctcgGGATCCggGAATTCgCAGATTTTCGTGAAAACCCTTAC	ampilfy ubiquitin from cDNAs
	ggaatttacgtaGCGGCCGCtCTCGAGTTAACCACCACGAAGTCTCAAC	
5. pMRX-IPU-muGFP-p62	ggttcaggctcgGGATCCggGAATTCgGCGTCGCTCACCGTGAAGGCC	ampilfy p62 from cDNAs
	tttacgtaGCGGCCGCtCTCGAGTCACAACGGCGGGGGATGCTTTG	
6. pMRX-IPU-muGFP-NDP52	ggttcaggctcgGGATCCggGAATTCgGAGGAGACCATCAAAGATCCCCC	ampilfy NDP52 from cDNAs
	ggaatttacgtaGCGGCCGCtTTACTCGAGaccTCAGAGAGAGTGGCAGAACACGTGG	
7. pMRX-IPU-muGFP-NBR1	ggttcaggctcgGGATCCggGAATTCgGAACCACAGGTTACTCTAAATGTGAC	ampilfy NBR1 from cDNAs
	ggaatttacgtaGCGGCCGCtTTACTCGAGaccTCAATAGCGTTGGCTGTACCAGTCG	
8. pMRX-IPU-muGFP-OPTN	ggttcaggctcgGGATCCggGAATTCgTCCCATCAACCTCTCAGCTGCCTCACTG	ampilfy OPTN from cDNAs
	ggaatttacgtaGCGGCCGCtTTACTCGAGaccTTAAATGATGCAATCCATCACGTGAATC	
9. pMRX-IPU-muGFP-TAX1BP1	ggttcaggctcgGGATCCggGAATTCgACATCCTTTCAAGAAGTCCC	ampilfy TAX1BP1 from cDNAs
	ggaatttacgtaGCGGCCGCtTTACTCGAGCTAGTCAAAATTTAGAACATTCTG	
10. pMRX-IPU-EGFP-ATG9A	ggccGGATCCGCGCAGTTTGACACTGAATACC	ampilfy ATG9A from cDNAs
	ggccGAATTCttaCTATACCTTGTGCACCTGAGGGGG	

Figures

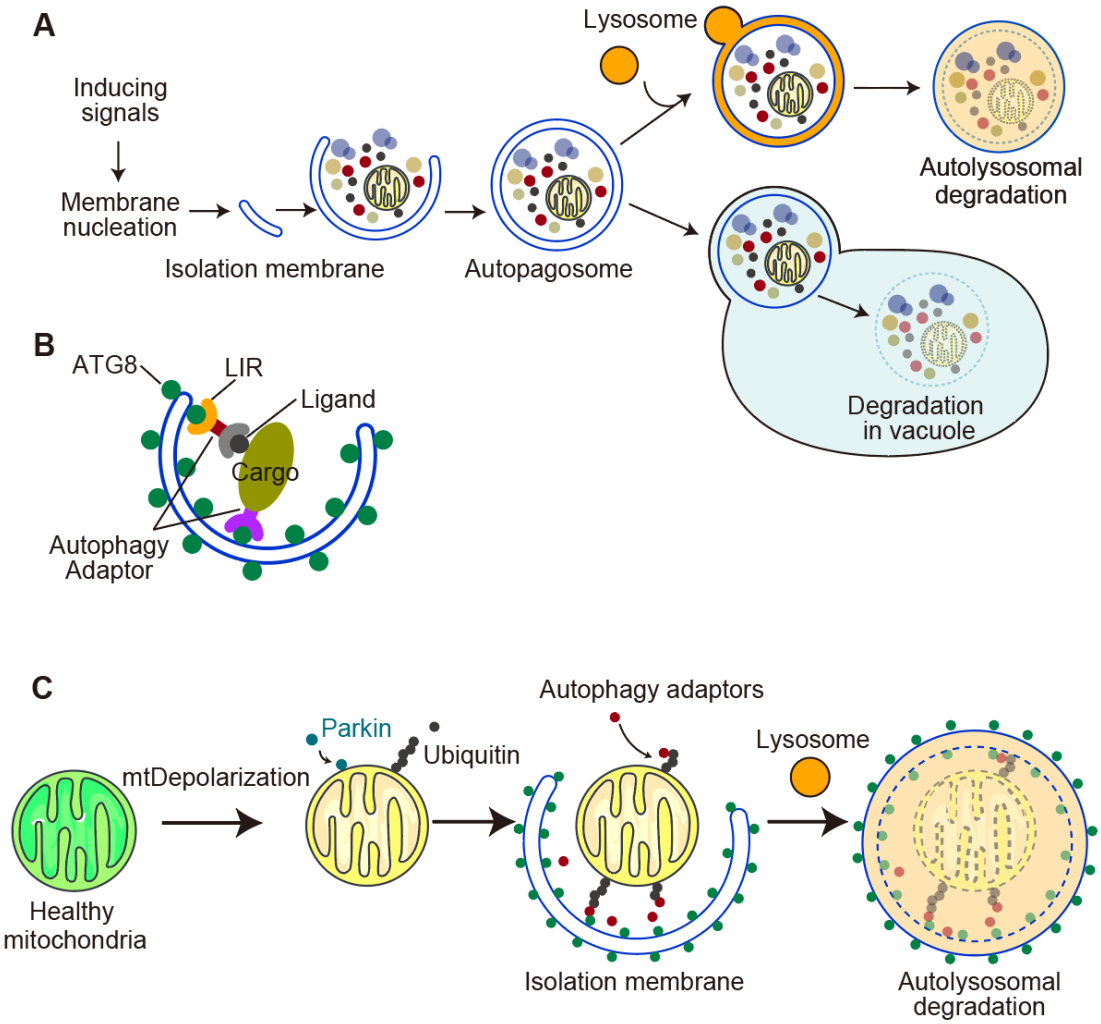

Figure. 1: Mechanism of autophagy.
(A) Overview of the process of autophagic degradation. After inducing, the isolation membrane is extended and closed to form autophagosomes, which surround proteins and organelles in the cytoplasm, and the autophagosomes fuse with lysosomes or delivered to vacuole to degrade the surrounding proteins and organelles.
(B) Molecular mechanism of cargo recognition in selective autophagy. Autophagy adaptors play a crucial role in linking cargoes to the autophagosome by interacting with ATG8 family proteins on the isolation membrane and either binding directly to cargoes or interact with ligands on the cargoes.
(C) Overview of the process of mitophagy. After mitochondria damage, Parkin is recruited and polyubiquitinates various mitochondrial outer membrane proteins and ubiquitinated proteins are recognized by several adaptors, leading to the recruitment of isolation membrane and subsequent degradation of the mitochondrion in autolysosome.

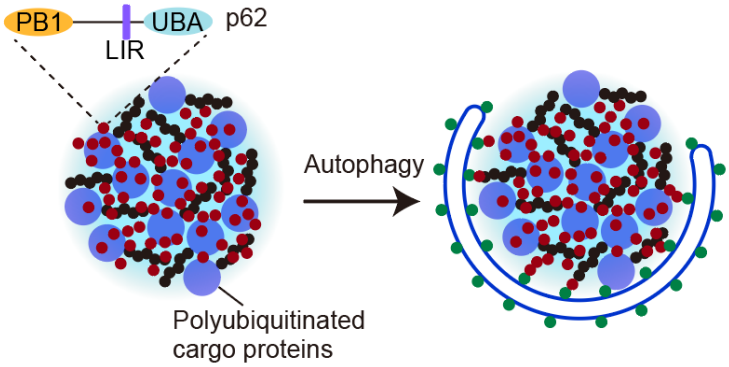

Figure 2. Phase separation of p62-polyubiquitinated protein aggregates.
LLPS mediates the assembly of condensates containing p62 and polyubiquitinated proteins. p62 polymerizes and interacts with ubiquitin to drive LLPS. In the condensates, p62 self-interacts via PB1 polymerization, while the polyubiquitinated proteins interact the p62 via ubiquitin–UBA domain interaction. Autophagosomal membranes selectively encase p62 aggregates through the interaction between p62's LIR domain and ATG8 family proteins locate on the isolation membrane.

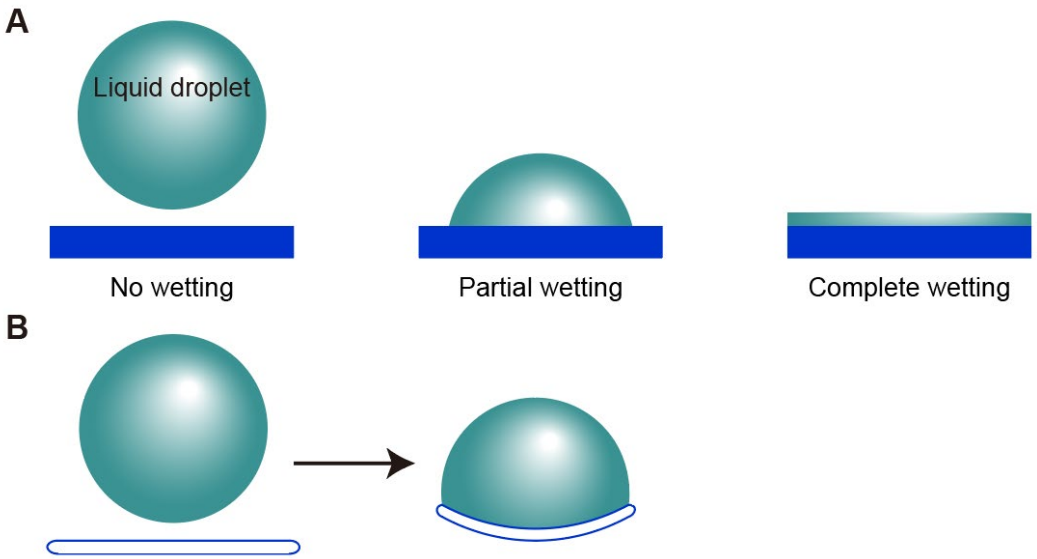

Figure 3. Wetting of different fluids and capillary force driving membrane deformation.

(A) Images shows a fluid with no wetting, partial wetting, or complete wetting. Wetting is a phenomenon that occurs at the interface between two materials, and it describes how the liquid interacts with the solid surface. No wetting occurs when a liquid does not spread or adhere to a solid surface. In this case, the liquid droplet forms a nearly spherical shape on the solid surface. Partial wetting occurs when a liquid partially wets or adheres to a solid surface. It forms a meniscus or droplet shape. Complete wetting occurs when a liquid fully wets and spreads across a solid surface, indicating strong adhesion and the formation of a flat and continuous liquid film on the solid.

(B) Deformation of membrane by capillary force. The liquid wets the membrane, causing it to spread and adhere to the membrane's surface. As the liquid wets the membrane, the capillary forces pull the liquid upward, causing the membrane to deform or bend.

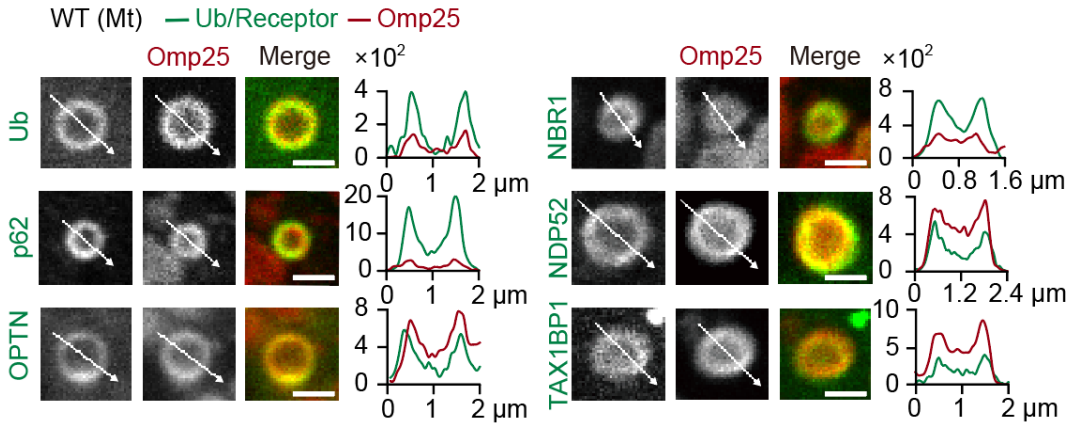

Figure 4. Autophagy adaptors show even distribution on separate mitochondria during Parkin-mediated mitophagy in WT HeLa cells.
Representative images (left) and spline graphs of the intensity profiles along the indicated lines in the respective images (right) of wild-type HeLa cells expressing one of the GFP-tagged autophagy adaptors or ubiquitin, mRuby–Omp25, and HaloTag7–LC3B at 45 min after 20 μM CCCP treatment. Separate mitochondria without contacting other mitochondria or isolation membranes (Mt) are shown. The y-axis in each of the graphs indicates the fluorescence intensity. Scale bars indicate 1 μm.

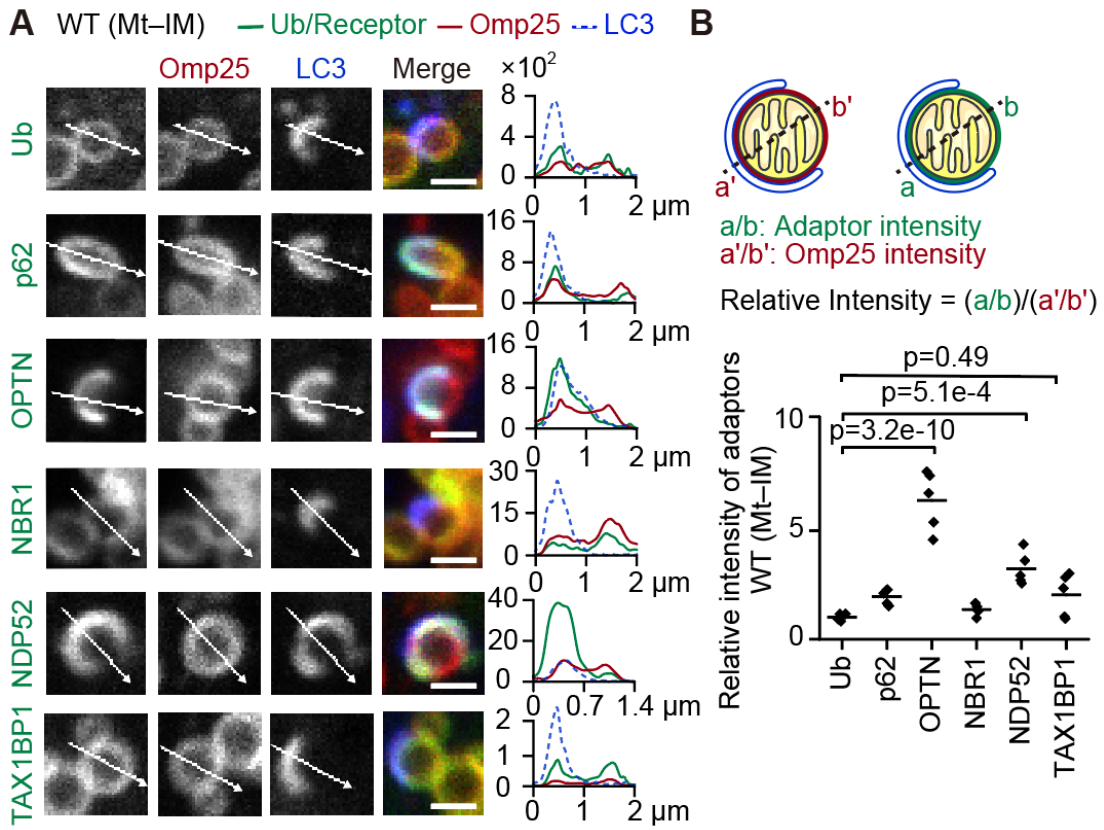

Figure 5. Autophagy adaptors distinct distributions on mitochondria with isolation membrane during Parkin-mediated mitophagy in WT HeLa cells.

(A) Representative images (left) and spline graphs of the intensity profiles along the indicated lines in the respective images (right) of wild-type HeLa cells expressing one of the GFP-tagged autophagy adaptors or ubiquitin, mRuby–Omp25, and HaloTag7–LC3B at 45 min after 20 μM CCCP treatment. Mitochondria with an isolation membrane (Mt–IM) are shown. The y-axis in each of the graphs indicates the fluorescence intensity. Scale bars indicate 1 μm.

(B) The relative intensity of GFP-tagged adaptors or ubiquitin (a and b) in LC3B-positive areas compared with LC3B-negative areas in panels B. GFP signals were normalized to the mRuby–Omp25 signals (a′ and b′) using the formula Relative Intensity = (a/b)/(a′/b′), where a and a′ represent the intensities in the LC3B-positive area, and b and b′ represent the intensities in the LC3B-negative area. Solid horizontal bars indicate the means, and dots indicate the data from five structures. Differences were statistically analyzed by one-way analysis of variance with Dunnett's post-hoc test.

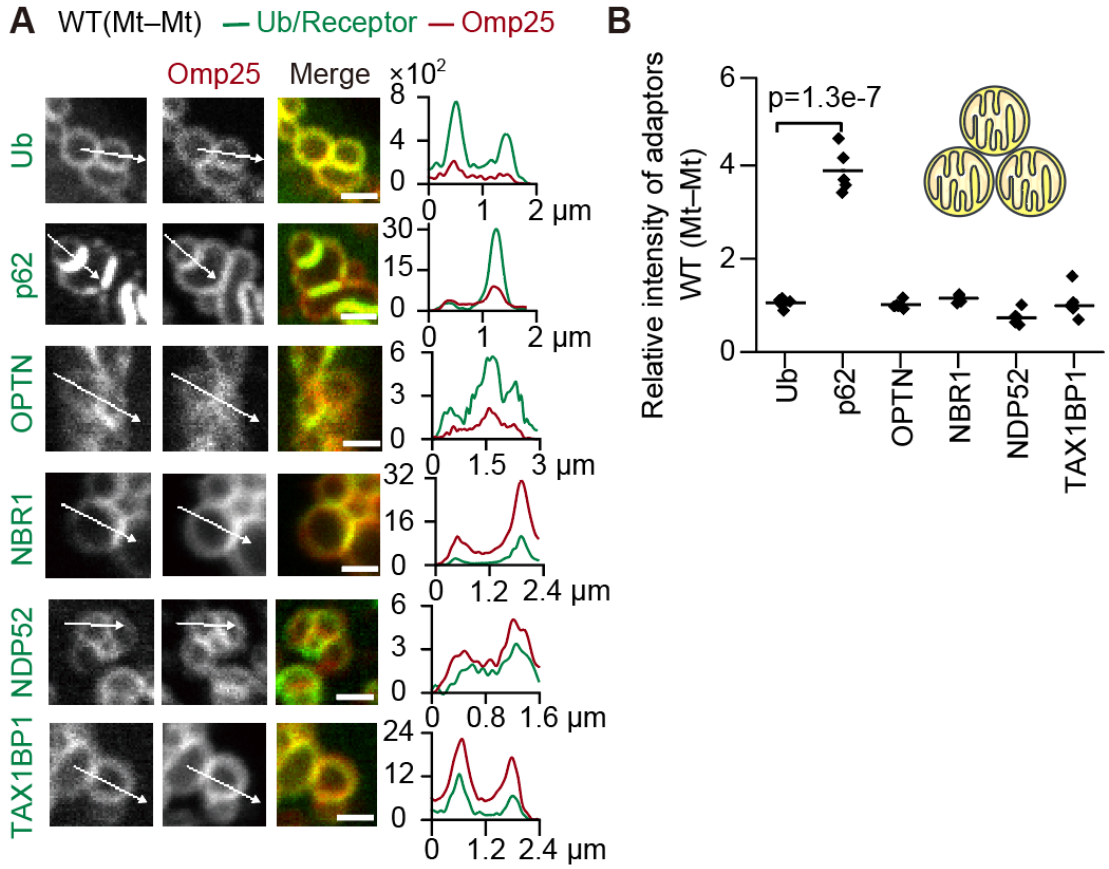

Figure 6. Autophagy adaptors distinct distributions on clustering mitochondria during Parkin-mediated mitophagy in WT HeLa cells.

(A) Representative images (left) and spline graphs of the intensity profiles along the indicated lines in the respective images (right) of wild-type HeLa cells expressing one of the GFP-tagged autophagy adaptors or ubiquitin, mRuby–Omp25, and HaloTag7–LC3B at 45 min after 20 µM CCCP treatment. Mitochondria contacting other mitchondria (Mt–Mt) are shown. The y-axis in each of the graphs indicates the fluorescence intensity. Scale bars indicate 1 µm.

(B) The relative intensity of each adaptor in Mt–IM was calculated as in Figure 3B. Solid bars indicate the means and dots indicate the data from 5 structures. Differences were statistically analyzed by one-way analysis with Dunnett's post hoc test.

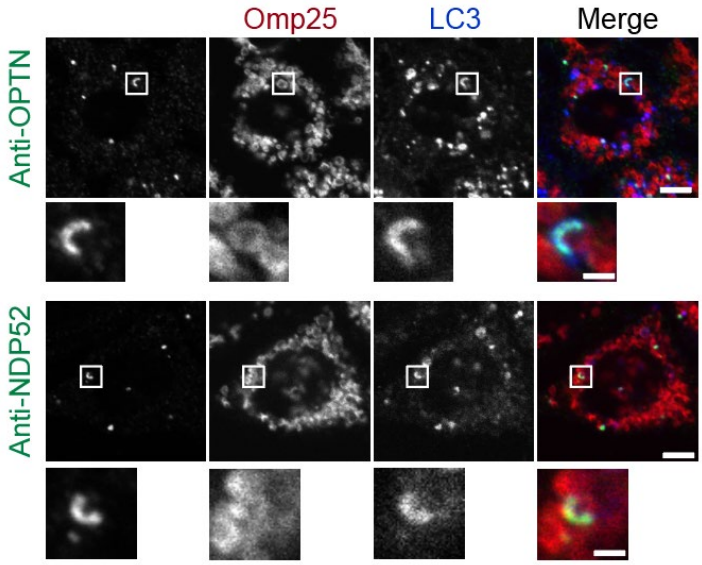

Figure 7. OPTN or NDP52 still accumulates to Mt–IM in wild-type HeLa cells. Immunostaining of endogenous OPTN or NDP52 in wild-type HeLa cells expressing mRuby–Omp25 and HaloTag7–LC3B at 45 min after 20 μM CCCP treatment. Scale bars indicate 4 μm and 1 μm (magnified images).

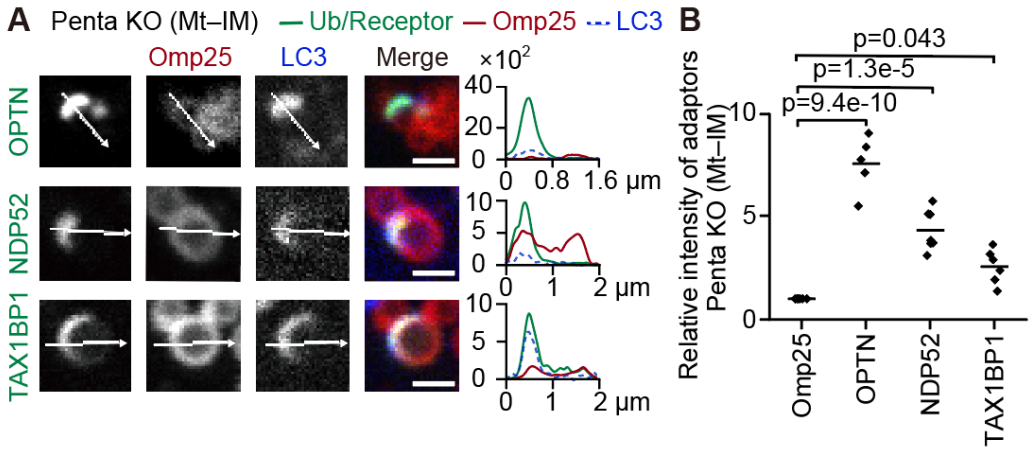

Figure 8. Autophagy adaptors show distinct distributions on mitochondria with isolation membrane during Parkin-mediated mitophagy in Penta KO cells.

(A) Representative images (left) and spline graphs of the intensity profiles along the indicated lines in the respective images (right) of HeLa cells lacking all five autophagy adaptors (penta KO cells) expressing one of the GFP-tagged autophagy adaptors or ubiquitin, mRuby–Omp25, and HaloTag7–LC3B at 45 min after 20 μM CCCP treatment. Mitochondria with an isolation membrane (Mt–IM) are shown. The y-axis in each of the graphs indicates the fluorescence intensity. Scale bars indicate 1 μm.

(B) The relative intensity of each adaptor in Mt–IM was calculated as in Figure 3B. Solid bars indicate the means and dots indicate the data from 5 structures. Differences were statistically analyzed by one-way analysis of variance with Dunnett's post-hoc test.

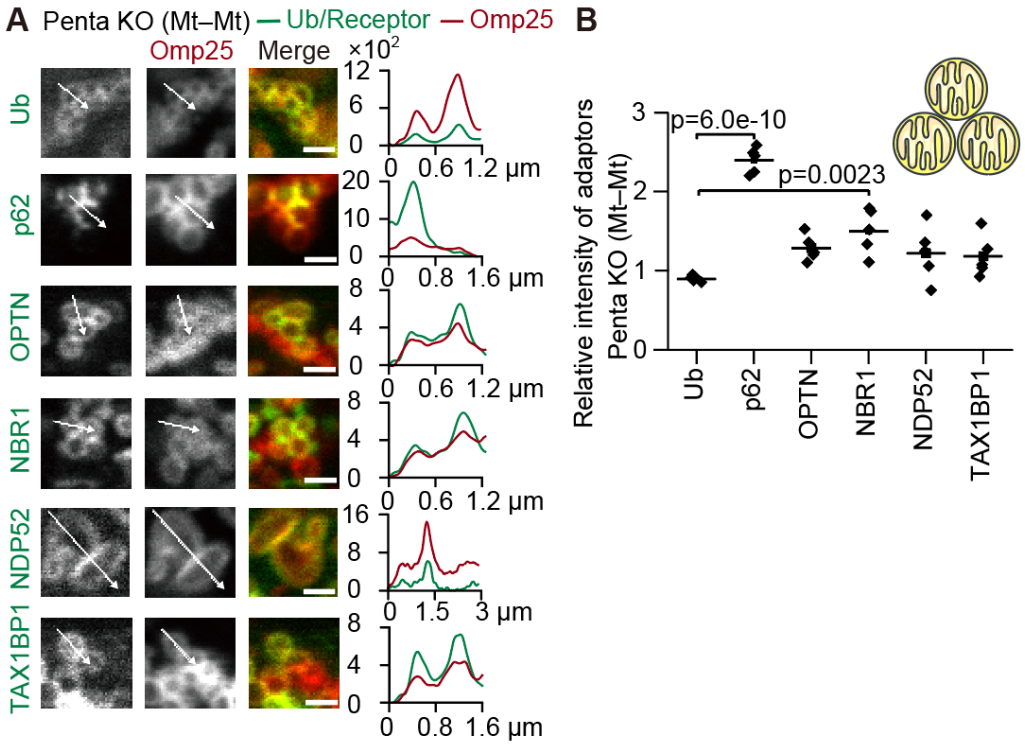

Figure 9. Autophagy adaptors show distinct distributions on clustering mitochondria during Parkin-mediated mitophagy in Penta KO cells.

(A) Representative images (left) and spline graphs of the intensity profiles along the indicated lines in the respective images (right) of HeLa cells lacking all five autophagy adaptors (penta KO cells) expressing one of the GFP-tagged autophagy adaptors or ubiquitin, mRuby–Omp25, and HaloTag7–LC3B at 45 min after 20 µM CCCP treatment. Accumulated mitochondria (Mt–Mt) are shown. The y-axis in each of the graphs indicates the fluorescence intensity. Scale bars indicate 1 µm.

(B) The relative intensity of each adaptor in Mt–Mt was calculated as in Figure 3B. Solid bars indicate the means and dots indicate the data from 5 structures. Differences were statistically analyzed by one-way analysis of variance with Dunnett's post-hoc test.

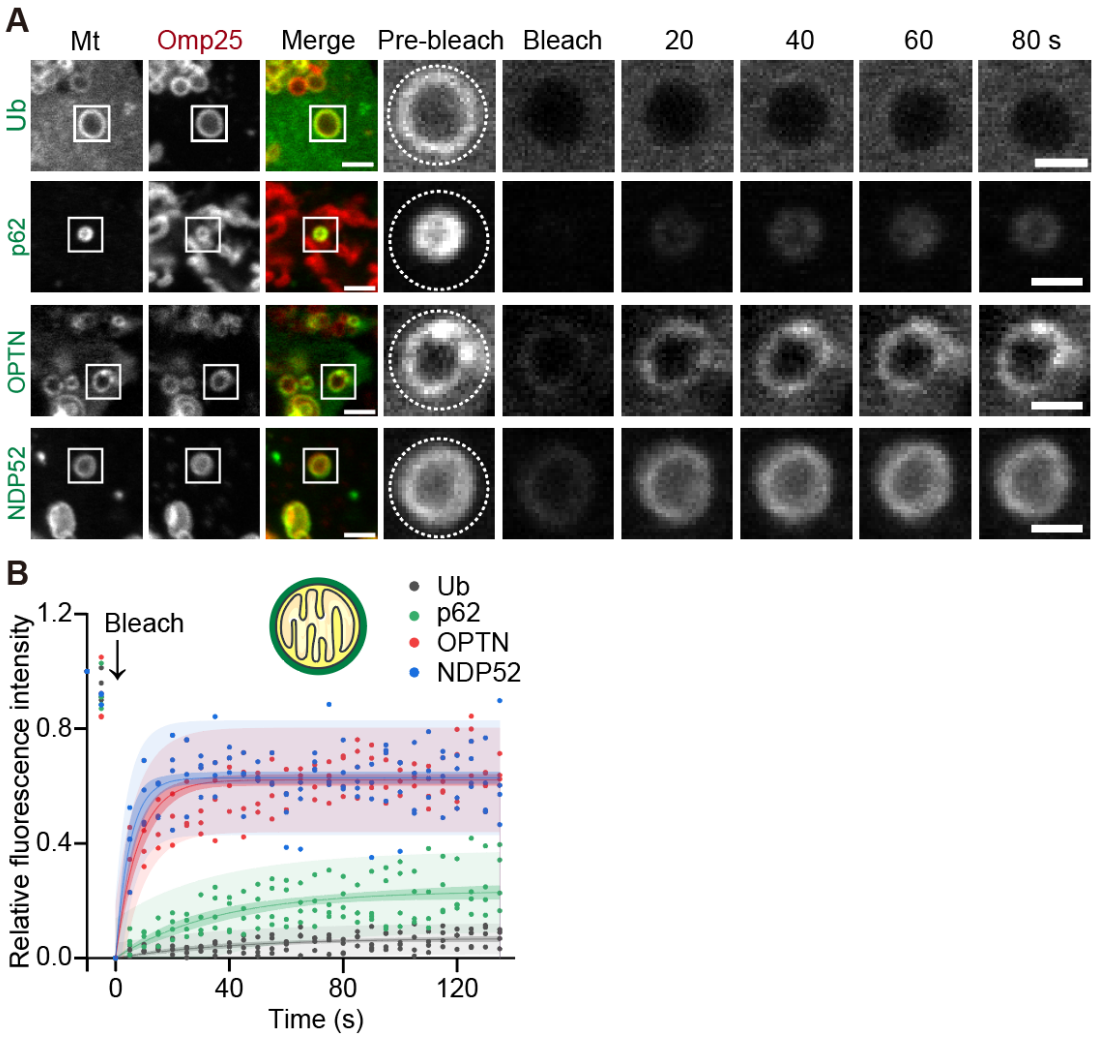

Figure 10. OPTN and NDP52 show a dynamic exchange between the mitochondrial surface and cytosol on separate mitochondria.

(A) Representative images of GFP fluorescence recovery after photobleaching (FRAP) on separate mitochondria (Mt) in HeLa cells lacking all five autophagy adaptors (penta KO cells) expressing GFP-tagged adaptors or ubiquitin at 45 min after 20 µM CCCP treatment. The photobleached areas are indicated by dotted lines. The magnified panels display time-lapse images of the photobleached areas. Scale bars indicate 2 µm and 1 µm (magnified images).

(B) Quantification of GFP fluorescence recovery after photobleaching (FRAP) on separate mitochondria (Mt) in HeLa cells lacking all five autophagy adaptors (penta KO cells) expressing GFP-tagged adaptors or ubiquitin at 45 min after 20 µM CCCP treatment. Data were collected from four structures and were fitted to the equation y = a*(1 − exp(−b*x)). The dark shaded areas represent the 95% confidence intervals, and the light shaded areas represent the 95% prediction intervals.

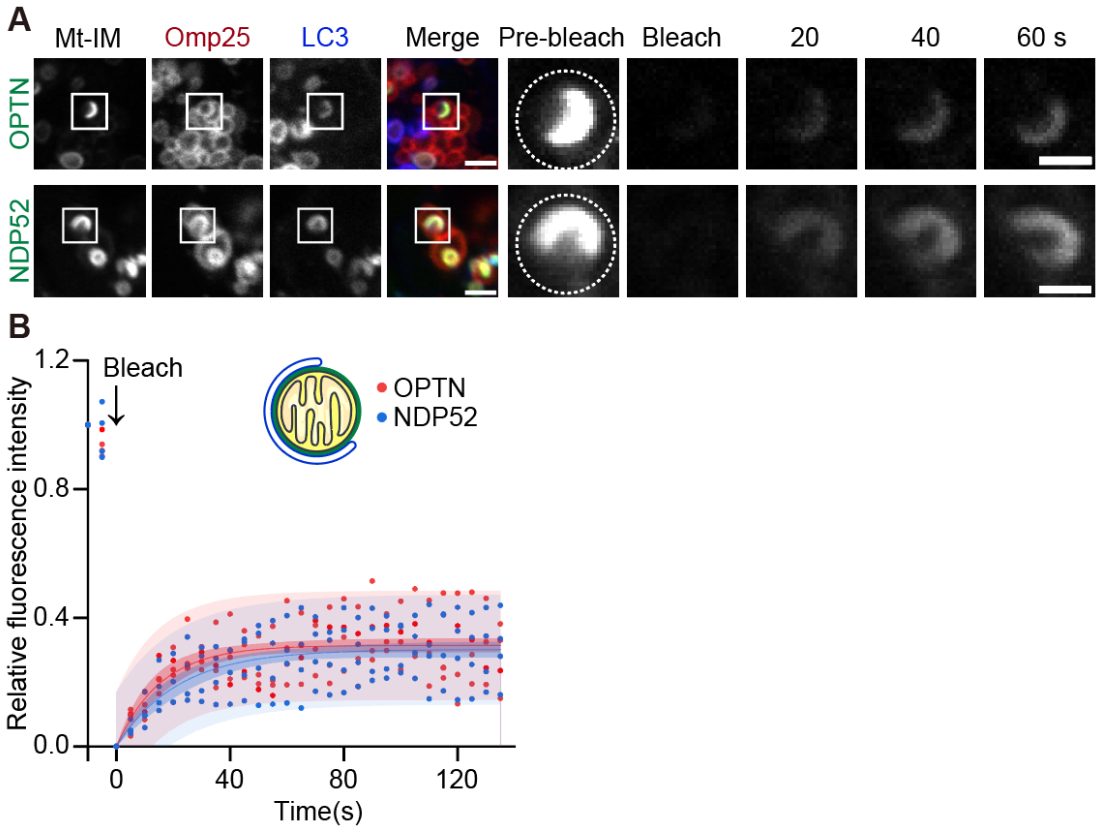

Figure 11. OPTN and NDP52 show a dynamic exchange between the mitochondrial surface and cytosol on mitochondria with an isolation membrane.
(A) Representative images of GFP fluorescence recovery after photobleaching (FRAP) on mitochondria with an isolation membrane (Mt–IM) in HeLa cells lacking all five autophagy adaptors (penta KO cells) expressing GFP-tagged adaptors or ubiquitin at 45 min after 20 μM CCCP treatment. The photobleached areas are indicated by dotted lines. The magnified panels display time-lapse images of the photobleached areas. Scale bars indicate 2 μm and 1 μm (magnified images).
(B) Quantification of GFP fluorescence recovery after photobleaching (FRAP) on mitochondria with an isolation membrane (Mt–IM) in HeLa cells lacking all five autophagy adaptors (penta KO cells) expressing GFP-tagged adaptors or ubiquitin at 45 min after 20 μM CCCP treatment. Data were collected from four structures and were fitted to the equation y = a*(1 − exp(−b*x)). The dark shaded areas represent the 95% confidence intervals, and the light shaded areas represent the 95% prediction intervals.

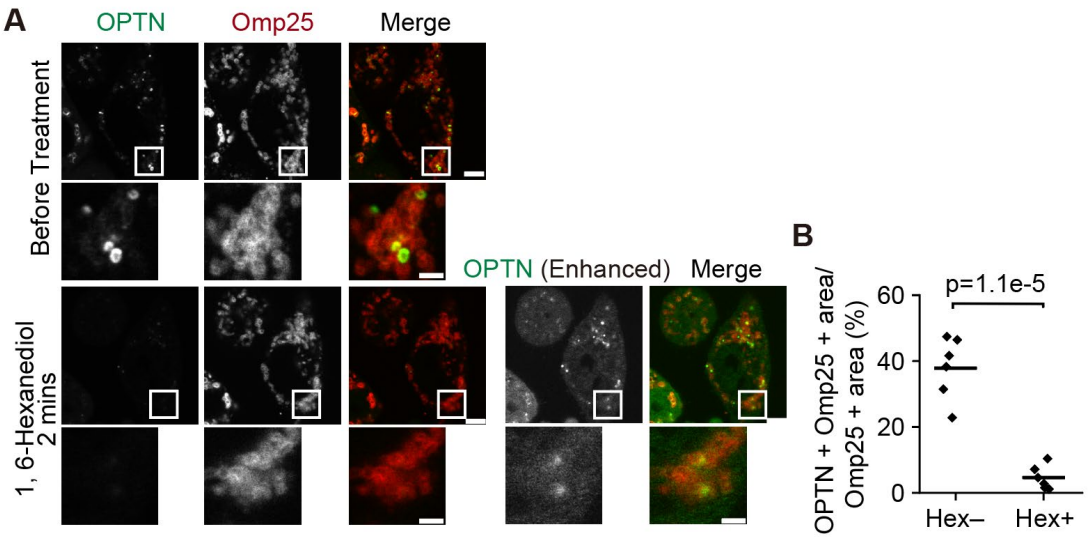

Figure 12. Accumulation of OPTN was dispersed by 1,6-hexanediol.

(A) Penta KO cells expressing GFP–OPTN at 45 min after 20 μM CCCP and 20 μM wortmannin treatment. Wortmannin was added to inhibit autophagosome formation so that OPTN would not be sequestered in a closed compartment. Images of cells before (upper panels) and 2 min after (lower panels) the addition of 10% 1,6-hexanediol are displayed. Scale bars indicate 5 μm and 2 μm (magnified images).

(B) Quantification of OPTN colocalization with mitochondria before and after 1,6-hexanediol treatment. Solid horizontal bars indicate the means, each dot indicates the mean value from one field of view with ≥5 cells (n=6). Differences were statistically analyzed by one-way analysis of variance with Dunnett's post-hoc test.

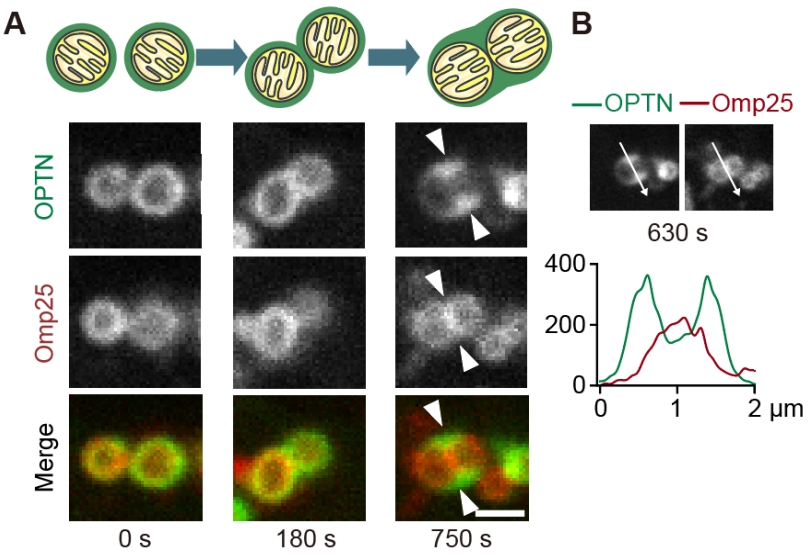

Figure 13. OPTN condensates redistribute upon two separate mitochondria with comparable sizes approaching and contacting each other.

(A) Time-lapse images of two separate mitochondria approaching and contacting each other. Events of the attachment of two mitochondria with comparable sizes was observed.

(B) Spline graphs of two separate mitochondria approaching and contacting each other. The line graphs represent the intensity profiles along the indicated lines in the respective images shown. The arrowheads indicate redistributed OPTN signals filling the cleft between two adjacent mitochondria. Scale bars indicate 1 μm.

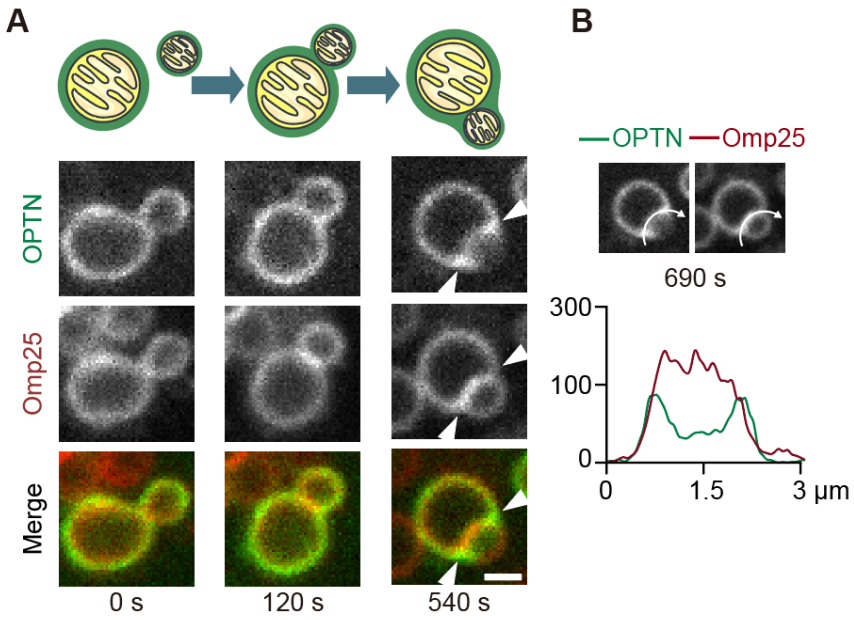

Figure 14. OPTN condensates redistribute upon two mitochondria with differing sizes approaching and contacting each other.

(A) Time-lapse images of two separate mitochondria approaching and contacting each other. Events of the attachment of two mitochondria with differing sizes were observed. (B) Spline graphs of two separate mitochondria approaching and contacting each other. The line graphs represent the intensity profiles along the indicated lines in the respective images shown. The arrowheads indicate redistributed OPTN signals filling the cleft between two adjacent mitochondria. Scale bars indicate 1 μm.

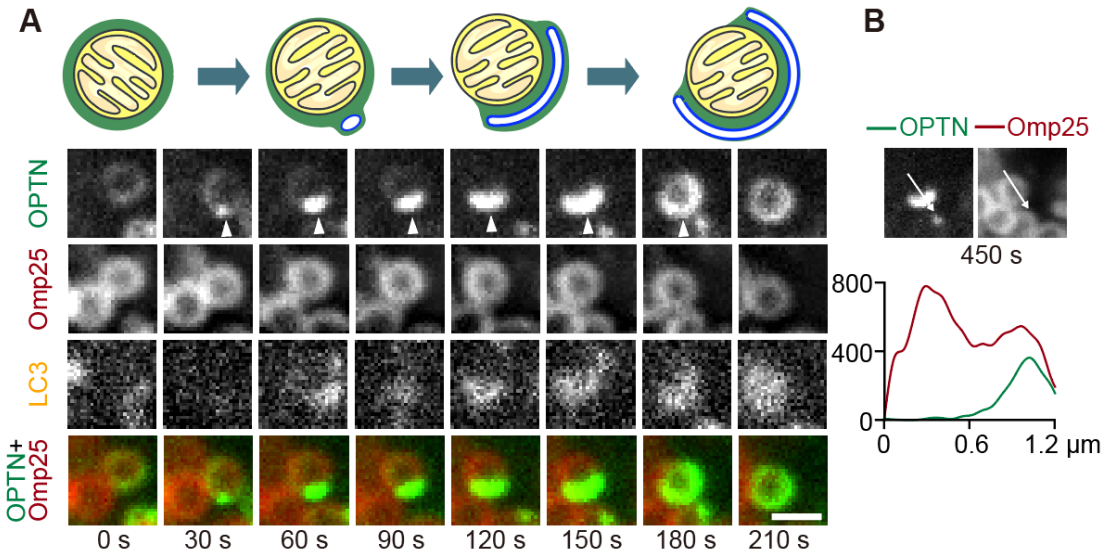

Figure 15. OPTN condensates redistribute upon contact with isolation membranes.
(A) Time-lapse images of a mitochondrion with an isolation membrane elongating on its surface. The arrowhead indicates the elongating isolation membrane.
(B) Spline graph of a mitochondrion with an isolation membrane elongating on its surface. The line graph represents the intensity profiles along the indicated lines in the respective images shown. Scale bars indicate 1 μm.

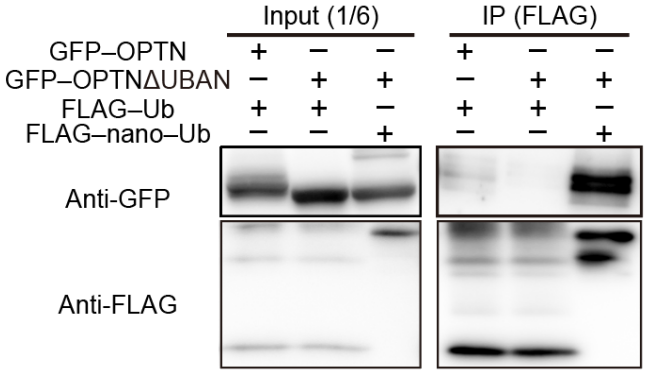

Figure 16. Anti-GFP nanobody shows enhanced binding affinity to GFP–OPTN. Interaction between GFP–OPTN mutants and FLAG–Ub or FLAG–nanobody–Ub was investigated by immunoprecipitation with an anti-FLAG antibody and immunoblotting with an anti-GFP antibody.

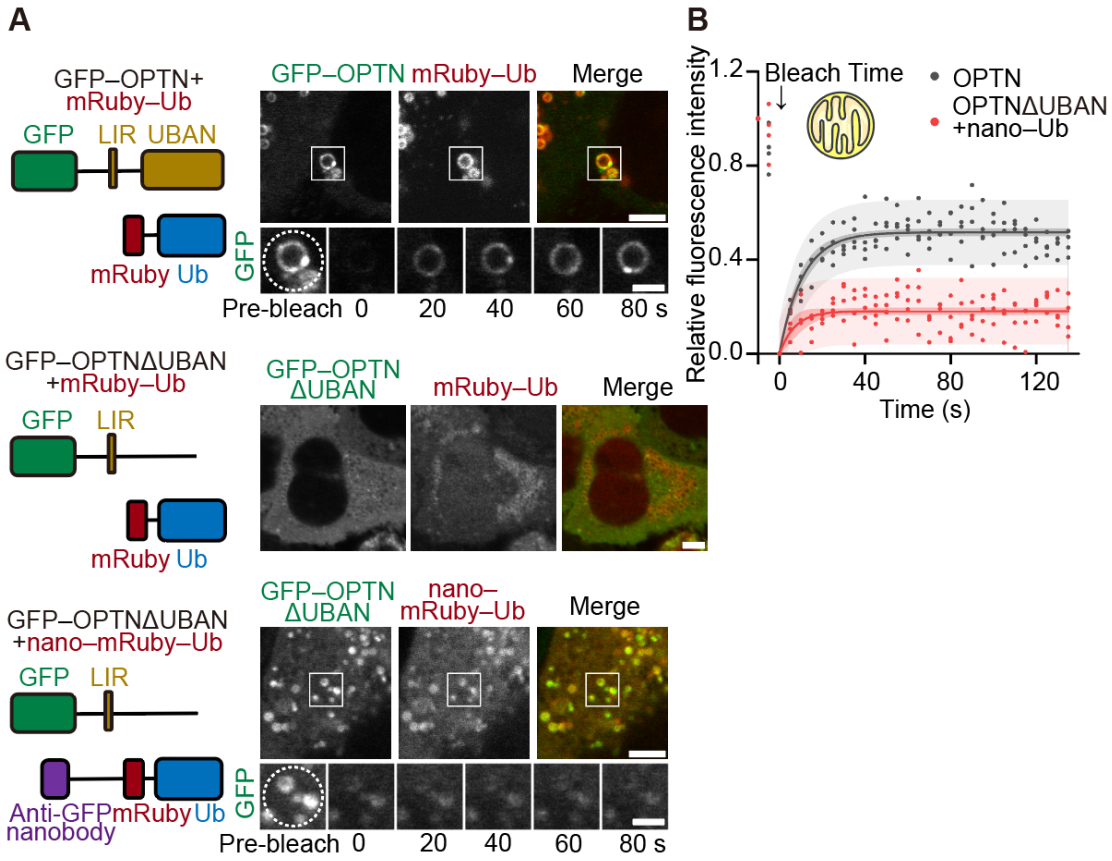

Figure 17. Dynamic exchange was inhibited by anti–GFP–nanobody.

(A) HeLa cells lacking all five autophagy adaptors (penta KO cells) expressing both GPF–OPTN and mRuby–Ub (top), both GFP–OPTNΔUBAN and mRuby–Ub (middle), or both GFP–OPTNΔUBAN and anti-GFP nanobody–mRuby–Ub (bottom) at 45 min after 20 μM CCCP treatment. Time-lapse images of GFP FRAP are shown. Photobleached areas are circled by dotted lines. Scale bars indicate 4 μm and 2 μm (magnified images).

(B) Quantification of GFP FRAP on separate mitochondria (Mt) in penta KO cells expressing both GFP–OPTN and mRuby–Ub or both GFP–OPTNΔUBAN and anti-GFP nanobody–mRuby–Ub at 45 min after 20 μM CCCP treatment. Data were collected from four structures and were fitted to the equation y = a*(1 − exp(−b*x)). The dark shading represents the 95% confidence intervals, and the light shading represent the 95% prediction intervals.

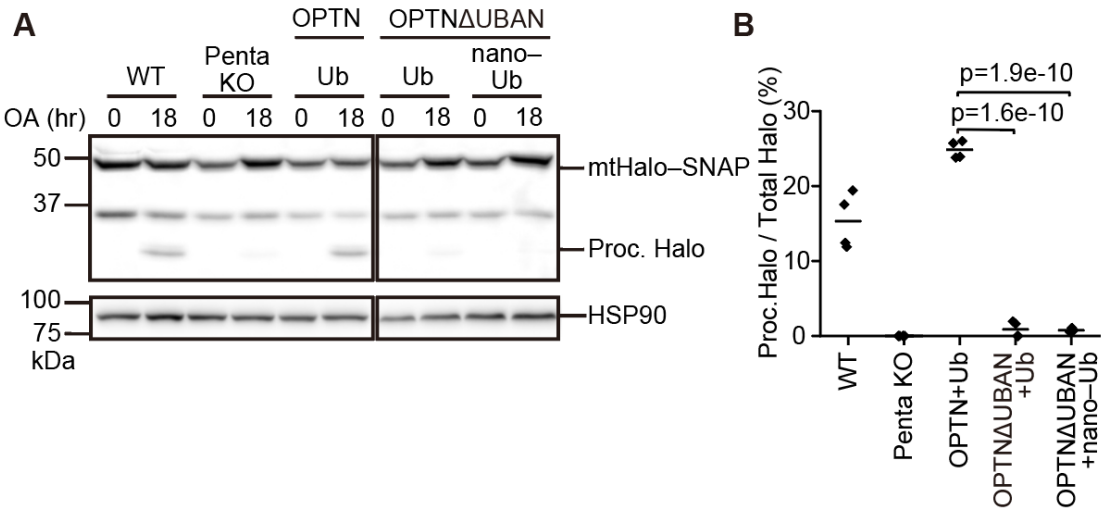

Figure 18. GFP–OPTNΔUBAN co-expressing with nanobody–mRuby–-Ub failed to restore mitophagy.

(A) Representative data of HaloTag (Halo) processing assay using cells expressing the indicated OPTN and Ub constructs. Cells expressing the mtHalo–SNAP mitophagy reporter were treated without (0 h) and with 1 μM oligomycin and 2 μM antimycin for 18 h. The amount of processed Halo (proc. Halo) indicates the relative amount of mitochondria degraded by the lysosomes.

(B) Quantification of HaloTag (Halo) processing assay using cells expressing the indicated OPTN and Ub constructs. Solid horizontal bars indicate the means, and dots indicate the data from four independent experiments. Differences were statistically analyzed by one-way analysis of variance with Dunnett's post-hoc test.

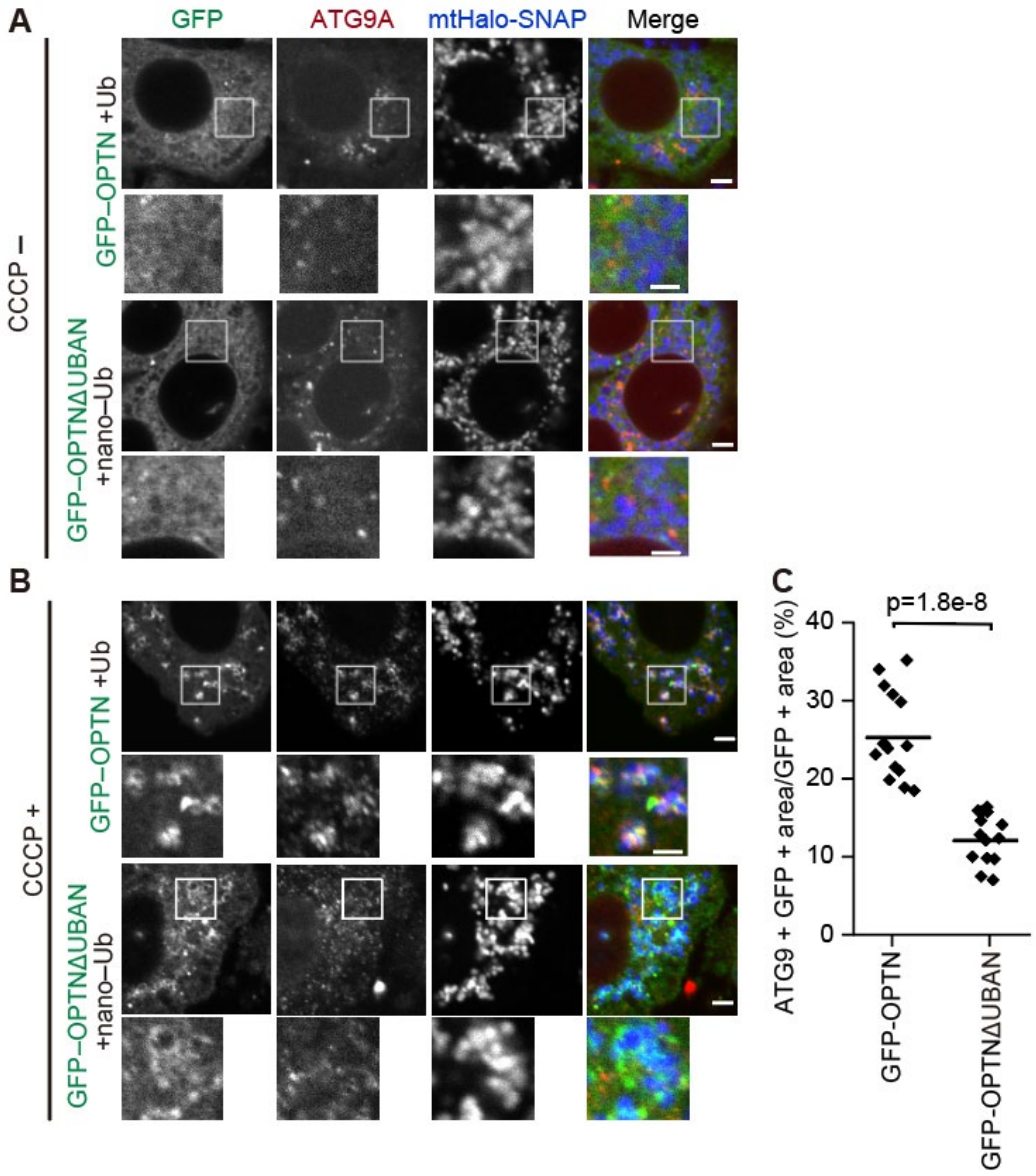

Figure 19. Liquid-like property of OPTN condensates is required for the recruitment of ATG9 vesicles.

(A and B) Localization of ATG9 vesicles under normal (CCCP−) (A) or mitophagy-inducing conditions (CCCP+, 60 min) (B). Endogenous ATG9 was immunostained in penta KO cells expressing both GFP–OPTN and mRuby–Ub or both GFP–OPTNΔUBAN and mRuby–nanobody–Ub together with mitochondrially targeted Halo–SNAP (mtHalo–SNAP). Scale bars indicate 4 μm and 2 μm (magnified images). (C) Quantification of ATG9A colocalization with mitochondria. Solid horizontal bars indicate the means, each dot indicates the mean value from one field of view with ≥10 cells (n=15). Differences were statistically analyzed by one-way analysis of variance with Dunnett's post-hoc test.

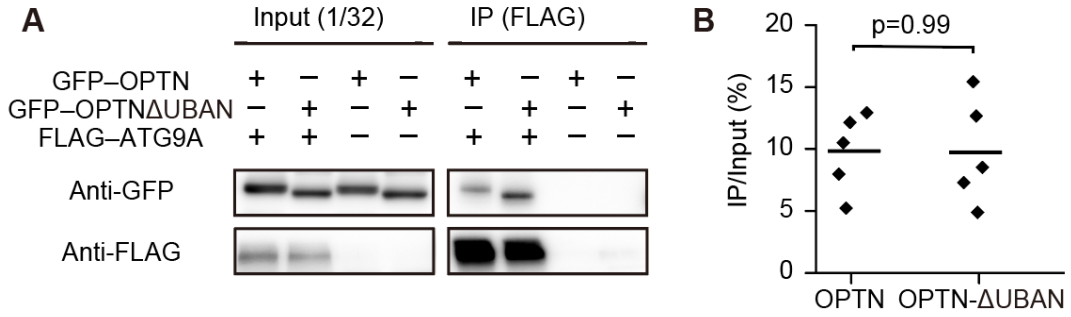

Figure 20. GFP–OPTNΔUBAN still retains the ATG9A-interacting domain and the ability to bind with the ATG9 vesicles.

(A) Representative data and quantification of organelle immunoprecipitation in cells expressing GFP–OPTN or GFP–OPTNΔUBAN in the presence or absence of FLAG-ATG9A. ATG9 vesicles were immunoprecipitated by FLAG M2 beads and GFP was blotted to detect the interaction between GFP–OPTN (WT or ΔUBAN) and ATG9 vesicles at 60 min after 20 μM CCCP treatment.

(B) Quantification of organelle immunoprecipitation in cells expressing GFP–OPTN or GFP–OPTNΔUBAN in the presence or absence of FLAG-ATG9A. Solid horizontal bars indicate the means, and dots indicate the data from five independent experiments. Differences were statistically analyzed by one-way analysis of variance with Dunnett's post-hoc test.

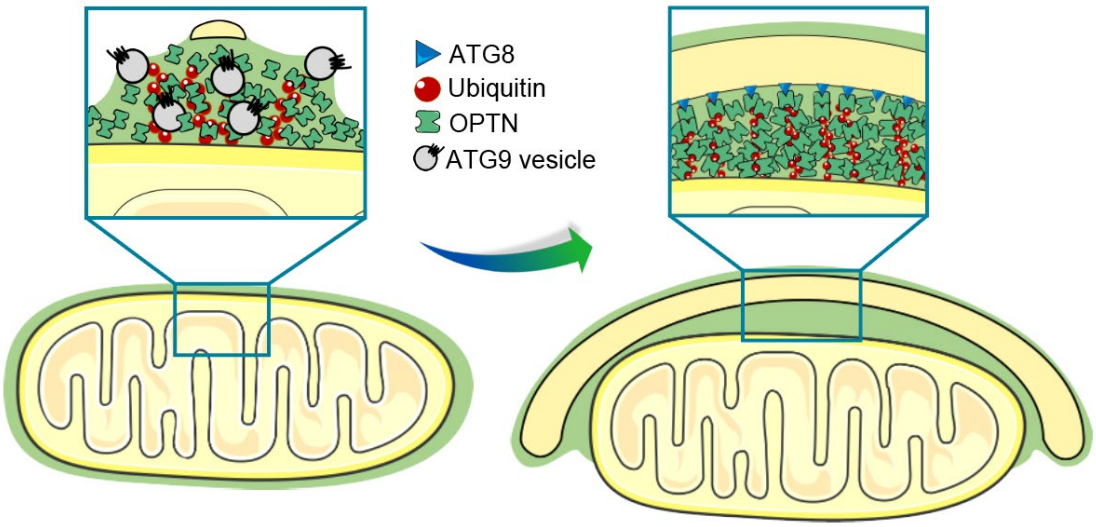

Figure 21. The models of ATG9 vesicle recruitment (left) and isolation membrane elongation (right) mediated by liquid-like OPTN condensates.
Partial or complete wetting of phase-separated OPTN enables the recruitment of ATG9 vesicles to ubiquitinated mitochondria (left). Wetting of OPTN on mitochondria and isolation membranes also facilitates the engulfment of mitochondria by the isolation membranes (right).

Acknowledgements

I would like to express my deepest gratitude to the following individuals and organizations for their invaluable support and contributions to the completion of this Ph.D. thesis. I would like to acknowledge the support and guidance provided by Professor Noboru Mizushima in shaping my academic and research path. I am immensely thankful to my advisor, Noboru Mizushima, Saori Yoshii, Haruka Chino and Roland L. Knorr, for their unwavering guidance, mentorship, and expertise. Their commitment to my academic and professional growth has been a constant source of inspiration. I am grateful to Saori Yoshii and Haruka Chino who have been part of this research journey. Their diverse perspectives and collective efforts have enriched this thesis. Many thanks to Haruka Chino for her care, guidance, and assistance to me when I first arrived in the laboratory and for her guidance and help with experiments. I am also grateful to the Japanese Ministry of Education, Culture, Sports, Science and Technology for providing me with a scholarship to pursue my graduate studies in Japan. To my wife Zhao Huan, your unwavering support, love, and encouragement have sustained me throughout this challenging endeavor. I am profoundly grateful for everything you have done for me. My friends, both near and far, have been a constant source of motivation and relief. Your companionship and understanding during the ups and downs of this journey have meant the world to me.

This journey has been long and challenging, but it has been made infinitely more manageable due to the unwavering support of these individuals.